

Antigen-Specific Antibody Design via Direct Energy-based Preference Optimization

Xiangxin Zhou^{*123} Dongyu Xue^{*3} Ruizhe Chen^{*43} Zaixiang Zheng³ Liang Wang¹² Quanquan Gu³

Abstract

Antibody design, a crucial task with significant implications across various disciplines such as therapeutics and biology, presents considerable challenges due to its intricate nature. In this paper, we tackle antigen-specific antibody design as a protein sequence-structure co-design problem, considering both rationality and functionality. Leveraging a pre-trained conditional diffusion model that jointly models sequences and structures of complementarity-determining regions (CDR) in antibodies with equivariant neural networks, we propose *direct energy-based preference optimization* to guide the generation of antibodies with both rational structures and considerable binding affinities to given antigens. Our method involves fine-tuning the pre-trained diffusion model using a residue-level decomposed energy preference. Additionally, we employ gradient surgery to address conflicts between various types of energy, such as attraction and repulsion. Experiments on RAbD benchmark show that our approach effectively optimizes the energy of generated antibodies and achieves state-of-the-art performance in designing high-quality antibodies with low total energy and high binding affinity, demonstrating the superiority of our approach.

1 Introduction

Antibodies, vital proteins with an inherent Y-shaped structure in the immune system, are produced in response to an immunological challenge. Their primary function is to discern and neutralize specific pathogens, typically referred to

^{*}Equal contribution ¹School of Artificial Intelligence, University of Chinese Academy of Sciences ²Center for Research on Intelligent Perception and Computing (CRIPAC), State Key Laboratory of Multimodal Artificial Intelligence Systems (MAIS), Institute of Automation, Chinese Academy of Sciences (CASIA) ³ByteDance Research (this work was done during Xiangxin and Ruizhe’s internship at ByteDance Research) ⁴College of Computer Science and Electronic Engineering, Hunan University. Correspondence to: Quanquan Gu <quanquan.gu@bytedance.com>.

Preprint. Copyright 2024 by the author(s).

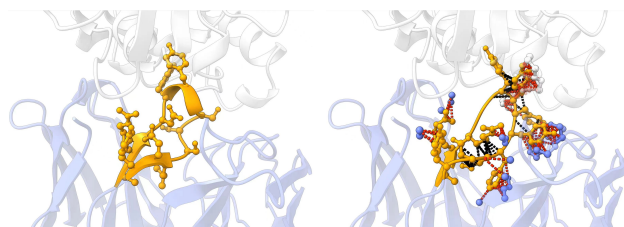


Figure 1. The third CDR in the heavy chain, CDR-H3 (colored in yellow), of real antibody (left) and synthetic antibody (right) designed by MEAN (Kong et al., 2023a) for a given antigen (PDB ID: 4cmh). The rest parts of antibodies except CDR-H3 are colored in blue. The antigens are colored in gray. We use red (resp. black) dotted lines to represent clashes between a CDR-H3 atom and a framework/antigen atom (resp. another CDR-H3 atom). We consider a clash occurs when the overlap of the van der Waals radii of two atoms exceeds 0.6Å.

as antigens, with a significant degree of specificity (Murphy & Weaver, 2016). The specificity mainly comes from the Complementarity Determining Regions (CDRs), which accounts for most binding affinity to specific antigens (Jones et al., 1986; Ewert et al., 2004; Xu & Davis, 2000; Akbar et al., 2021). Hence, the design of CDRs is a crucial step in developing potent therapeutic antibodies, which plays an important role in drug discovery.

Traditional *in silico* antibody design methods rely on sampling or searching protein sequences over a large search space to optimize the physical and chemical energy, which is inefficient and easily trapped in bad local minima (Adolf-Bryfogle et al., 2018; Lapidoth et al., 2015; Warszawski et al., 2019). Recently, deep generative models have been employed to model protein sequences in nature for antibody design (Alley et al., 2019; Ferruz et al., 2022). Following the fundamental biological principle that structure determines function numerous efforts have been focused on antibody sequence-structure co-design (Jin et al., 2022b;a; Luo et al., 2022; Kong et al., 2023a;b; Martinkus et al., 2023), which demonstrate superiority over sequence design-based methods. However, the main evaluation metrics in the aforementioned works are amino acid recovery (AAR) and root mean square deviation (RMSD) between the generated antibody and the real one. This is controversial because AAR is susceptible to manipulation and does not precisely gauge the quality of the generated antibody sequence. Mean-

while, RMSD does not involve side chains, which are vital for antigen-antibody interaction. Besides, it is biologically plausible that a specific antigen can potentially bind with multiple efficacious antibodies (Victora & Nussenzweig, 2012; Dong et al., 2021). This motivates us to examine the generated structures and sequences of antibodies through the lens of energy, which reflects the rationality of the designed antibodies and their binding affinity to the target antigens. We have noted that nearly all antibody sequence-structure co-design methods struggle to produce antibodies with low energy. This suggests the presence of irrational structures and inadequate binding affinity in antibodies designed by these methods (see Fig. 1). We attribute this incapability to the insufficient model training caused by a scarcity of high-quality data.

To tackle the above challenges and bridge the gap between *in silico* antibody sequence-structure co-design methods and the intrinsic need for drug discovery, we formulate the antibody design task as an antibody optimization problem with a focus on better rationality and functionality. Inspired by direct preference optimization (DPO, Rafailov et al., 2023) and self-play fine-tuning techniques (Chen et al., 2024) that achieve huge success in the alignment of large language models (LLMs), we proposed a direct energy-based preference optimization method named ABDPO for antibody optimization. More specifically, we first pre-train a conditional diffusion model on real antigen-antibody datasets, which simultaneously captures sequences and structures of complementarity-determining regions (CDR) in antibodies with equivariant neural networks. We then progressively fine-tune this model using synthetic antibodies generated by the model itself given an antigen with energy-based preference. This preference is defined at a fine-grained residue level, which promotes the effectiveness and efficiency of the optimization process. To fulfill the requirement of both rationality and functionality, we decompose the energy into multiple types so that we can incorporate prior knowledges and mitigate the interference between conflicting energy types (e.g., repulsion and attraction) to guide the optimization process. Fine-tuning with self-synthesized energy-based antibody preference data represents a revolutionary solution to address the limitation of scarce high-quality real-world data, a significant challenge in this domain. We highlight our main contributions as follows:

- We tackle the antibody sequence-structure co-design problem through the lens of energy from the perspectives of both rationality and functionality.
- We propose direct residue-level energy-based preference optimization to fine-tune diffusion models for designing antibodies with rational structures and high binding affinity to specific antigens.
- We introduce energy decomposition and conflict mitigation techniques to enhance the effectiveness and efficiency of the optimization process.

- Experiments show that ABDPO outperforms the state-of-the-art baselines by a large margin in generating antibodies with low total energy and high binding ability to the target antigen, resembling natural antibodies.

2 Related Work

Antibody Design. The application of deep learning to antibody design can be traced back to at least (Liu et al., 2020; Saka et al., 2021; Akbar et al., 2022). In recent years, sequence-structure co-design of antibodies has attracted increasing attention. Jin et al. (2022b) proposed to simultaneously design sequences and structures of CDRs in an autoregressive way and iteratively refine the designed structures. Jin et al. (2022a) further utilized the epitope and focused on designing CDR-H3 with a hierarchical message passing equivariant network. Kong et al. (2023a) incorporated antigens and the light chains of antibodies as conditions and designed CDRs with E(3)-equivariant graph networks via a progressive full-shot scheme. Luo et al. (2022) proposed a diffusion model that takes residue types, atom coordinates and side-chain orientations into consideration to generate antigen-specific CDRs. Kong et al. (2023b) focused on epitope-binding CDR-H3 design and modelled full-atom geometry. Recently, Martinkus et al. (2023) proposed Ab-Diffuser, a novel diffusion model for antibody design, that incorporates more domain knowledge and physics-based constraints and also enables side-chain generation. Besides, Wu & Li (2023); Gao et al. (2023) and Zheng et al. (2023) introduced pre-trained protein language model to antibody design. Distinct from the above works, our method places a stronger emphasis on designing and optimizing antibodies with low energy and high binding affinity.

Alignment of Generative Models. Solely maximizing the likelihood of training data does not always lead to a model that satisfies users’ preferences. Recently, many efforts have been made on the alignment of the generative models to human preferences. Reinforcement learning has been introduced to learning from human/AI feedback to large language models, such as RLHF (Ouyang et al., 2022) and RLAIF (Lee et al., 2023). Typically, RLHF consists of three phases: supervised fine-tuning, reward modeling, and RL fine-tuning. Similar ideas have also been introduced to text-to-image generation, such as DDPO (Black et al., 2023), DPOR (Fan et al., 2023) and DiffAC (Zhou et al., 2024). They view the generative processes of diffusion models as a multi-step Markov Decision Process (MDP) and apply policy gradient for fine-tuning. Rafailov et al. (2023) proposed direct preference optimization (DPO) to directly fine-tune language models on preference data, which matches RLHF in performance. Recently, DPO has been introduced to text-to-image generation (Wallace et al., 2023; Anonymous, 2023). Notably, in the aforementioned works, models pre-trained with large-scale datasets have already shown strong performance, in which case alignment fur-

ther increases users’ satisfaction. In contrast, in our work, the model pre-trained with limited real-world antibody data is insufficient in performance. Therefore, preference optimization in our case is primarily used to help the model understand the essence of nature and meet the requirement of antibody design.

3 Method

In this section, we present ABDPO, a direct energy-based preference optimization method for designing antibodies with reasonable rationality and functionality (Fig. 2). We first define the antibody generation task and introduce the diffusion model for this task in Sec. 3.1. Then we introduce residue-level preference optimization for fine-tuning the diffusion model and analyze its advantages in effectiveness and efficiency in Sec. 3.2. Finally, in Sec. 3.3, we introduce the energy decomposition and describe how to mitigate the conflicts when optimizing multiple types of energy.

3.1 Preliminaries

We focus on designing CDR-H3 of the antibody given antigen structure as CDR-H3 contributes the most to the diversity and specificity of antibodies (Xu & Davis, 2000; Akbar et al., 2021) and the rest part of the antibody including the frameworks and other CDRs. Following Luo et al. (2022), each amino acid is represented by its type $s_i \in \{\text{ACDEFGHIKLMNPQRSTVWY}\}$, C_α coordinate $\mathbf{x}_i \in \mathbb{R}^3$, and frame orientation $\mathbf{O}_i \in \text{SO}(3)$ (Kofinas et al., 2021), where $i = 1, \dots, N$ and N is the number of the amino acids in the protein complex. We assume the CDR-H3 to be generated has m amino acids, which can be denoted by $\mathcal{R} = \{(s_j, \mathbf{x}_j, \mathbf{O}_j) | j = l + 1, \dots, l + m\}$. The rest part of the antigen-antibody complex can be denoted by $\mathcal{P} = \{(s_i, \mathbf{x}_i, \mathbf{O}_i) | i \in \{1, \dots, N\} \setminus \{l + 1, \dots, l + m\}\}$. The antibody generation task can be then formulated as modeling the conditional distribution $P(\mathcal{R} | \mathcal{P})$.

Denosing Diffusion Probabilistic Model (DDPM, Ho et al., 2020) have been introduced to antibody generation by Luo et al. (2022). This approach consists of a forward *diffusion* process and a reverse *generative* process. The diffusion process gradually injects noises into data as follows:

$$\begin{aligned} q(s_j^t | s_j^0) &= \mathcal{C}(\mathbf{1}(s_j^t) | \bar{\alpha}^t \mathbf{1}(s_j^0) + \bar{\beta}^t \mathbf{1}/K), \\ q(\mathbf{x}_j^t | \mathbf{x}_j^0) &= \mathcal{N}(\mathbf{x}_j^t | \sqrt{\bar{\alpha}^t} \mathbf{x}_j^0, \bar{\beta}^t \mathbf{I}), \\ q(\mathbf{O}_j^t | \mathbf{O}_j^0) &= \mathcal{IG}_{\text{SO}(3)}(\mathbf{O}_j^t | \text{ScaleRot}(\sqrt{\bar{\alpha}^t} \mathbf{O}_j^0), \bar{\beta}^t), \end{aligned}$$

where $(s_j^0, \mathbf{x}_j^0, \mathbf{O}_j^0)$ are the noisy-free amino acid at time step 0 with index j , and $(s_j^t, \mathbf{x}_j^t, \mathbf{O}_j^t)$ are the noisy amino acid at time step t . $\{\beta^t\}_{t=1}^T$ is the noise schedule for the diffusion process (Ho et al., 2020), and we define $\bar{\alpha}^t = \prod_{\tau=1}^t (1 - \beta^\tau)$ and $\bar{\beta}^t = 1 - \bar{\alpha}^t$. K is the number of amino acid types. Here, $\mathcal{C}(\cdot)$, $\mathcal{N}(\cdot)$, $\mathcal{IG}_{\text{SO}(3)}(\cdot)$ are categorical distribution, Gaussian distribution on \mathbb{R}^3 , and isotropic Gaussian distribution on $\text{SO}(3)$ (Leach et al., 2022) respectively. `ScaleRot` scales the rotation angle with fixed rotation axis to modify the

rotation matrix (Gallier & Xu, 2003).

Correspondingly, the reverse generative process learns to recover data by iterative denoising. The denoising process $p(\mathcal{R}^{t-1} | \mathcal{R}^t, \mathcal{P})$ from time step t to time step $t - 1$ is defined as follows:

$$p(s_j^{t-1} | \mathcal{R}^t, \mathcal{P}) = \mathcal{C}(s_j^{t-1} | \mathbf{f}_{\theta_1}(\mathcal{R}^t, \mathcal{P})[j]), \quad (1)$$

$$p(\mathbf{x}_j^{t-1} | \mathcal{R}^t, \mathcal{P}) = \mathcal{N}(\mathbf{x}_j^{t-1} | \mathbf{f}_{\theta_2}(\mathcal{R}^t, \mathcal{P})[j], \beta^t \mathbf{I}), \quad (2)$$

$$p(\mathbf{O}_j^{t-1} | \mathcal{R}^t, \mathcal{P}) = \mathcal{IG}_{\text{SO}(3)}(\mathbf{f}_{\theta_3}(\mathcal{R}^t, \mathcal{P})[j], \beta^t), \quad (3)$$

where $\mathcal{R}^t = \{s_j, \mathbf{x}_j, \mathbf{O}_j\}_{j=l+1}^{l+m}$ is the noisy sequence and structure of CDR-H3 at time step t , \mathbf{f}_{θ_1} , \mathbf{f}_{θ_2} , \mathbf{f}_{θ_3} are parameterized by SE(3)-equivariant neural networks (Jing et al., 2021; Jumper et al., 2021). $\mathbf{f}(\cdot)[j]$ denotes the output that corresponds to the j -th amino acid. The training objective of the reverse generative process is to minimize the Kullback–Leibler (KL) divergence between variational distribution p and the posterior distribution q as follows:

$$L = \mathbb{E}_{\mathcal{R}^t \sim q} \left[\frac{1}{m} \sum_{j=l+1}^{l+m} \mathbb{D}_{\text{KL}} \left(q(\mathcal{R}^{t-1}[j] | \mathcal{R}^t, \mathcal{P}) \parallel p_{\theta}(\mathcal{R}^{t-1}[j] | \mathcal{R}^t, \mathcal{P}) \right) \right]. \quad (4)$$

With some algebra, we can simplify the above objective and derive the reconstruction loss at time step t as follows:

$$L_s^t = \mathbb{E}_{\mathcal{R}^t} \left[\frac{1}{m} \sum_{j=l+1}^{l+m} \mathbb{D}_{\text{KL}} \left(q(s_j^{t-1} | s_j^0, s_j^0) \parallel p(s_j^{t-1} | \mathcal{R}^t, \mathcal{P}) \right) \right], \quad (5)$$

$$L_x^t = \mathbb{E}_{\mathcal{R}^t} \left[\frac{1}{m} \sum_{j=l+1}^{l+m} \|\mathbf{x}_j^0 - \mathbf{f}_{\theta_2}(\mathcal{R}^t, \mathcal{P})\|^2 \right], \quad (6)$$

$$L_O^t = \mathbb{E}_{\mathcal{R}^t} \left[\frac{1}{m} \sum_{j=l+1}^{l+m} \|(\mathbf{O}_j^0)^T \mathbf{f}_{\theta_3}(\mathcal{R}^t, \mathcal{P}) - \mathbf{I}\|_F^2 \right], \quad (7)$$

where $\mathcal{R}^t \sim q(\mathcal{R}^t | \mathcal{R}^0)$ and $\mathcal{R}^0 \sim P(\mathcal{R} | \mathcal{P})$, and $\|\cdot\|_F$ is the matrix Frobenius norm. Note that as Luo et al. (2022) mentioned, Eqs. (1) and (3) are an empirical perturbation-denosing process instead of a rigorous one. Thus the terminology *KL-divergence* may not be proper for orientation \mathbf{O} . Nevertheless, we can still approximately derive an empirical reconstruction loss for orientation \mathbf{O} as above that works in practice. The overall loss is $L \approx \mathbb{E}_{t \sim U[1, T]} [L_s^t + L_x^t + L_O^t]$. After optimizing this loss, we can start with the noises from the prior distribution and then apply the reverse process to generate antibodies.

3.2 Direct Energy-based Preference Optimization

Only the antibodies with considerable sequence-structure rationality and binding affinity can be used as effective therapeutic candidates. Fortunately, these two properties can be estimated by biophysical energy. Thus, we introduce direct energy-based preference optimization to fine-tune the pre-trained diffusion models for antibody design.

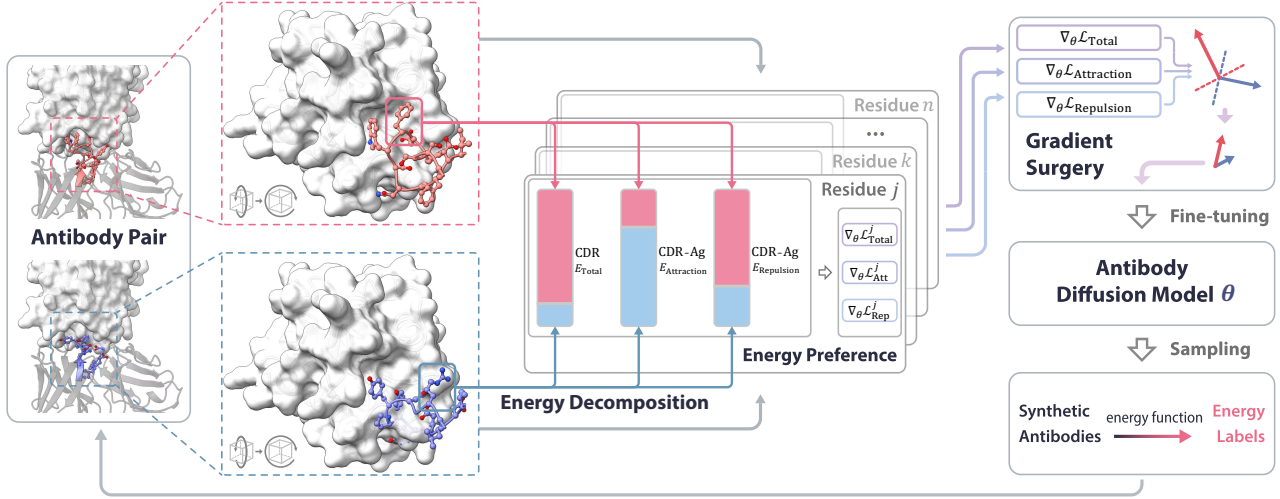


Figure 2. Overview of ABDPO. This process can be summarized as: (a) Generate antibodies using the pre-trained diffusion model; (b) Evaluate the residue-level multiple types of energy and construct preference data; (c) Compute the losses for energy-based preference optimization and mitigate the conflicts between losses of multiple types of energy; (d) Update the diffusion model with the merged loss.

Inspired by RLHF (Ouyang et al., 2022), we can fine-tune the pre-trained model to maximize the reward as:

$$\max_{p_{\theta}} \mathbb{E}_{\mathcal{R}^0 \sim p_{\theta}} [r(\mathcal{R}^0)] - \beta \mathbb{D}_{\text{KL}}(p_{\theta}(\mathcal{R}^0) \| p_{\text{ref}}(\mathcal{R}^0)),$$

where p_{θ} (resp. p_{ref}) is the distribution induced by the model being fine-tuned (resp. the fixed pre-trained model), β is a hyperparameter that controls the Kullback–Leibler (KL) divergence regularization. The optimal solution to the above objective takes the form:

$$p_{\theta^*}(\mathcal{R}^0) = \frac{1}{Z} p_{\text{ref}}(\mathcal{R}^0) \exp\left(\frac{1}{\beta} r(\mathcal{R}^0)\right).$$

Following Rafailov et al. (2023), we turn to the DPO objective as follows:

$$L_{\text{DPO}} = -\mathbb{E}_{\mathcal{R}_w^0, \mathcal{R}_l^0} \left[\log \sigma \left(\beta \log \frac{p_{\theta}(\mathcal{R}_w^0)}{p_{\text{ref}}(\mathcal{R}_w^0)} - \beta \log \frac{p_{\theta}(\mathcal{R}_l^0)}{p_{\text{ref}}(\mathcal{R}_l^0)} \right) \right],$$

where $\sigma(\cdot)$ is sigmoid, \mathcal{R}_w^0 and \mathcal{R}_l^0 are “winning” and “losing” data pair (i.e., $\mathcal{R}_w^0 \succ \mathcal{R}_l^0$) sampled from the Bradley-Terry (BT, Bradley & Terry, 1952) model with reward $r(\cdot)$, i.e., $p(\mathcal{R}_1^0 \succ \mathcal{R}_2^0) = \sigma(r(\mathcal{R}_1^0) - r(\mathcal{R}_2^0))$. Please refer to Appendix C for more detailed derivations.

Due to the intractable $p_{\theta}(\mathcal{R}^0)$, following Wallace et al. (2023), we introduce latent variables $\mathcal{R}^{1:T}$ and utilize the evidence lower bound optimization (ELBO). In particular, L_{DPO} can be modified as follows:

$$L_{\text{DPO-Diffusion}} = -\mathbb{E}_{\mathcal{R}_w^0, \mathcal{R}_l^0} \left[\log \sigma \left(\beta \mathbb{E}_{\mathcal{R}_w^{1:T}, \mathcal{R}_l^{1:T}} \left[\log \frac{p_{\theta}(\mathcal{R}_w^{0:T})}{p_{\text{ref}}(\mathcal{R}_w^{0:T})} - \log \frac{p_{\theta}(\mathcal{R}_l^{0:T})}{p_{\text{ref}}(\mathcal{R}_l^{0:T})} \right] \right) \right],$$

where $\mathcal{R}_w^{1:T} \sim p_{\theta}(\mathcal{R}_w^{1:T} | \mathcal{R}_w^0)$ and $\mathcal{R}_l^{1:T} \sim p_{\theta}(\mathcal{R}_l^{1:T} | \mathcal{R}_l^0)$.

Following Wallace et al. (2023), we can utilize Jensen’s inequality and convexity of function $-\log \sigma$ to derive the following upper bound of $L_{\text{DPO-Diffusion}}$:

$$\tilde{L}_{\text{DPO-Diffusion}} = -\mathbb{E}_{t, \mathcal{R}_w^0, \mathcal{R}_l^0, (\mathcal{R}_w^{t-1}, \mathcal{R}_w^t), (\mathcal{R}_l^{t-1}, \mathcal{R}_l^t)} \left[\log \sigma \left(\beta T \log \frac{p_{\theta}(\mathcal{R}_w^{t-1} | \mathcal{R}_w^t)}{p_{\text{ref}}(\mathcal{R}_w^{t-1} | \mathcal{R}_w^t)} - \beta T \log \frac{p_{\theta}(\mathcal{R}_l^{t-1} | \mathcal{R}_l^t)}{p_{\text{ref}}(\mathcal{R}_l^{t-1} | \mathcal{R}_l^t)} \right) \right],$$

where $t \sim \mathcal{U}(0, T)$, $(\mathcal{R}_w^{t-1}, \mathcal{R}_w^t)$ and $(\mathcal{R}_l^{t-1}, \mathcal{R}_l^t)$ are sampled from reverse generative process of \mathcal{R}_w^0 and \mathcal{R}_l^0 , respectively, i.e., $(\mathcal{R}_w^{t-1}, \mathcal{R}_w^t) \sim p_{\theta}(\mathcal{R}_w^{t-1}, \mathcal{R}_w^t | \mathcal{R}_w^0)$ and $(\mathcal{R}_l^{t-1}, \mathcal{R}_l^t) \sim p_{\theta}(\mathcal{R}_l^{t-1}, \mathcal{R}_l^t | \mathcal{R}_l^0)$.

In our case, the antibodies with low energy are desired. Thus, we define the reward $r(\cdot)$ as $-\mathcal{E}(\cdot)/\mathcal{T}$, where $\mathcal{E}(\cdot)$ is the energy function and \mathcal{T} is the temperature. Different from the text-to-image generation where the (latent) reward is assigned to a complete image instead of a pixel (Wallace et al., 2023), we know more fine-grained credit assignment. Specifically, it is known that $\mathcal{E}(\mathcal{R}^0) = \sum_{j=l+1}^{l+m} \mathcal{E}(\mathcal{R}^0[j])$, i.e., the energy of an antibody is the summation of the energy of its amino acids (Alford et al., 2017). Thus the preference can be measured at the residue level instead of the entire CDR level. Besides, we have $\log p_{\theta}(\mathcal{R}^{t-1} | \mathcal{R}^t) = \sum_{j=l+1}^{l+m} \log p_{\theta}(\mathcal{R}^{t-1}[j] | \mathcal{R}^t)$. Thus, by Jensen’s inequality and the convexity of $-\log \sigma$, we can further derive the residue-level preference optimization loss, which is an upper bound of $\tilde{L}_{\text{DPO-Diffusion}}$:

$$L_{\text{Residue-DPO-Diffusion}} = -\mathbb{E}_{t, \mathcal{R}_w^0, \mathcal{R}_l^0, (\mathcal{R}_w^{t-1}, \mathcal{R}_w^t), (\mathcal{R}_l^{t-1}, \mathcal{R}_l^t)} \left[\sum_{j=l+1}^{l+m} \log \sigma \left(\beta T \log \frac{p_{\theta}(\mathcal{R}_w^{t-1}[j] | \mathcal{R}_w^t)}{p_{\text{ref}}(\mathcal{R}_w^{t-1}[j] | \mathcal{R}_w^t)} - \beta T \log \frac{p_{\theta}(\mathcal{R}_l^{t-1}[j] | \mathcal{R}_l^t)}{p_{\text{ref}}(\mathcal{R}_l^{t-1}[j] | \mathcal{R}_l^t)} \right) \right].$$

The gradients of $\tilde{L}_{\text{DPO-Diffusion}}$ and $L_{\text{residue-DPO-Diffusion}}$ with respect to the parameters θ can be written as:

$$\begin{aligned} \nabla_{\theta} \tilde{L}_{\text{DPO-Diffusion}} = & -\beta T \mathbb{E}_{t, \mathcal{R}_w^0, \mathcal{R}_l^0, t-1, t \sim p_{\theta}} \left[\right. \\ & \sum_{j=l+1}^{l+m} \sigma(\hat{r}(\mathcal{R}_l^0) - \hat{r}(\mathcal{R}_w^0)) \cdot \\ & \left. (\nabla_{\theta} \log p_{\theta}(\mathcal{R}_w^{t-1}[j] | \mathcal{R}_w^t) - \nabla_{\theta} \log p_{\theta}(\mathcal{R}_l^{t-1}[j] | \mathcal{R}_l^t)) \right], \end{aligned}$$

and

$$\begin{aligned} \nabla_{\theta} L_{\text{residue-DPO-Diffusion}} = & -\beta T \mathbb{E}_{t, \mathcal{R}_w^0, \mathcal{R}_l^0, t-1, t \sim p_{\theta}} \left[\right. \\ & \sum_{j=l+1}^{l+m} \sigma(\hat{r}(\mathcal{R}_l^0[j]) - \hat{r}(\mathcal{R}_w^0[j])) \cdot \\ & \left. (\nabla_{\theta} \log p_{\theta}(\mathcal{R}_w^{t-1}[j] | \mathcal{R}_w^t) - \nabla_{\theta} \log p_{\theta}(\mathcal{R}_l^{t-1}[j] | \mathcal{R}_l^t)) \right], \end{aligned}$$

where $\hat{r}(\cdot) := \log(p_{\theta}(\cdot)/p_{\text{ref}}(\cdot))$, which can be viewed as the estimated reward by current policy p_{θ} and $\mathcal{R}_w^0, \mathcal{R}_l^0, t-1, t \sim p_{\theta}$ denotes the following for brevity:

$$\begin{aligned} \mathcal{R}_w^0, \mathcal{R}_l^0 & \sim p_{\theta}(\mathcal{R}^0), \\ (\mathcal{R}_w^{t-1}, \mathcal{R}_w^t) & \sim p_{\theta}(\mathcal{R}_w^{t-1}, \mathcal{R}_w^t | \mathcal{R}_w^0), \\ (\mathcal{R}_l^{t-1}, \mathcal{R}_l^t) & \sim p_{\theta}(\mathcal{R}_l^{t-1}, \mathcal{R}_l^t | \mathcal{R}_l^0). \end{aligned}$$

We can see that $\nabla_{\theta} \tilde{L}_{\text{DPO-Diffusion}}$ actually reweight $\nabla_{\theta} \log p_{\theta}(\mathcal{R}^{t-1}[j] | \mathcal{R}^t)$ with the estimated reward of the complete antibody while $\nabla_{\theta} L_{\text{residue-DPO-Diffusion}}$ does this with the estimated reward of the amino acid itself. In this case, $\nabla_{\theta} \tilde{L}_{\text{DPO-Diffusion}}$ will increase (resp. decrease) the likelihood of all amino acids of the ‘‘winning’’ sample (resp. ‘‘losing’’) at the same rate, which may mislead the optimization direction. In contrast, $\nabla_{\theta} L_{\text{residue-DPO-Diffusion}}$ does not have this issue and can fully utilize the residue-level signals from estimated reward to effectively optimize antibodies.

We further approximate the objective $L_{\text{residue-DPO-Diffusion}}$ by sampling from the forward diffusion process q instead of the reverse generative process p_{θ} to achieve diffusion-like efficient training. With further replacing $\log \frac{p_{\theta}}{p_{\text{ref}}}$ with $-\log \frac{q}{p_{\theta}} + \log \frac{p_{\text{ref}}}{q}$ which is exactly $-\mathbb{D}_{\text{KL}}(q || p_{\theta}) + \mathbb{D}_{\text{KL}}(q || p_{\text{ref}})$ when taking expectation with respect to q , we can derive the final loss for fine-tuning the diffusion model as follows:

$$\begin{aligned} L_{\text{ABDPO}} = & -\mathbb{E}_{t, \mathcal{R}_w^0, \mathcal{R}_l^0, (\mathcal{R}_w^{t-1}, \mathcal{R}_w^t), (\mathcal{R}_l^{t-1}, \mathcal{R}_l^t)} \left[\right. \\ & \sum_{j=l+1}^{l+m} \log \sigma \left(-\beta T \{ \mathbb{D}_{\text{KL}}^{w,t}(q || p_{\theta})[j] - \mathbb{D}_{\text{KL}}^{w,t}(q || p_{\text{ref}})[j] \right. \\ & \left. \left. - \mathbb{D}_{\text{KL}}^{l,t}(q || p_{\theta})[j] + \mathbb{D}_{\text{KL}}^{l,t}(q || p_{\text{ref}})[j] \} \right) \right], \quad (8) \end{aligned}$$

where \mathcal{R}_w^0 and \mathcal{R}_l^0 are the ‘‘winning’’ and ‘‘losing’’ samples generated by the diffusion model, i.e., $\mathcal{R}_w^0, \mathcal{R}_l^0 \sim p_{\theta}(\mathcal{R})$, $(\mathcal{R}_w^{t-1}, \mathcal{R}_w^t)$ and $(\mathcal{R}_l^{t-1}, \mathcal{R}_l^t)$ are sampled from forward diffusion process of \mathcal{R}_w^0 and \mathcal{R}_l^0 , respectively, i.e., $(\mathcal{R}_w^{t-1}, \mathcal{R}_w^t) \sim q(\mathcal{R}_w^{t-1}, \mathcal{R}_w^t | \mathcal{R}_w^0)$ and $(\mathcal{R}_l^{t-1}, \mathcal{R}_l^t) \sim q(\mathcal{R}_l^{t-1}, \mathcal{R}_l^t | \mathcal{R}_l^0)$, which can be much more efficient than the

Algorithm 1 Direct Energy-based Preference Optimization

Input: pre-trained diffusion model parameter θ , the antigen-antibody complex except CDR-H3 \mathcal{P} , the number of iterations N_{outer} , the number of optimization steps per iteration N_{inner} sampling batch size B_{sample} , training batch size B_{train} , energy functions and their weights $\{(\mathcal{E}_v(\cdot), w_v)\}_{v=1}^V$, learning rate η

Output: model parameters θ , generated antibodies set \mathcal{D}

$\mathcal{D} \leftarrow \emptyset; \theta_{\text{ref}} \leftarrow \theta$

for $\tau = 1$ **to** N_{outer} **do**

 # Sample B_{sample} antibodies.

$\{\mathcal{R}_i\} \leftarrow \text{Generate}(\theta, \mathcal{P}, B_{\text{sample}})$

 # Evaluate the residue-level energy.

$\{\{\mathcal{E}_v(\mathcal{R}_i)[j]\}_{j=l+1, v=1}^{l+m, V}\} \leftarrow \text{Evaluate}(\{\mathcal{R}_i\})$

 # Append to the dataset.

$\mathcal{D} \leftarrow \mathcal{D} \cup \{(\mathcal{R}_i, \mathcal{E}_v(\mathcal{R}_i)[j])_{j=l+1, v=1}^{l+m, V}\}$

for $\nu = 1$ **to** N_{outer} **do**

 # Randomly construct B_{train} pairs of antibodies.

$\{(\mathcal{R}_w, \mathcal{R}_l)_i\} \leftarrow \text{SamplePairBatch}(\mathcal{D}, B_{\text{train}})$

 # Compute ABDPO loss as Eq. (8).

$\{L_v\} \leftarrow \text{ComputeEPOLoss}(\{(\mathcal{R}_w, \mathcal{R}_l)_i\}, \theta, \theta_{\text{ref}})$

 # Apply gradient surgery as Eq. (9).

$\{\nabla_{\theta} L_v\} \leftarrow \text{GradientSurgery}(\{\nabla_{\theta} L_v\})$

 # Update model parameters.

$\theta \leftarrow \theta - \eta \sum_{v=1}^V w_v \nabla_{\theta} L_v$

end for

end for

reverse generative process that involves hundreds of model forward estimation. Here we use $\mathbb{D}_{\text{KL}}^{w,t}(q || p_{\theta})[j]$ to denote $\mathbb{D}_{\text{KL}}(q(\mathcal{R}_w^{t-1}[j] | \mathcal{R}_w^{t-1}, \mathcal{R}^0) || p_{\theta}(\mathcal{R}_l^{t-1}[j] | \mathcal{R}^0))$. Similar for $\mathbb{D}_{\text{KL}}^{w,t}(q || p_{\text{ref}})[j]$, $\mathbb{D}_{\text{KL}}^{l,t}(q || p_{\theta})[j]$, and $\mathbb{D}_{\text{KL}}^{l,t}(q || p_{\text{ref}})[j]$. These KL divergence can be estimated as in Eqs. (5) to (7).

3.3 Energy Decomposition and Conflict Mitigation

The energy usually consists of different types, such as attraction and repulsion. Empirically, direct optimization on energy will lead to some undesired ‘‘shortcuts’’. Specifically, in some cases, repulsion dominate the energy of the antibody so the model will push antibodies as far from the antigen as possible to decrease the repulsion during optimization, and finally fall into a bad local minima. This effectively reduces the repulsion, but also completely eliminates the attraction between antibodies and antigens, which seriously impairs the functionality of the antibody. This motivates us to explicitly express the energy with several distinct terms and then control the optimization process towards our preference.

Inspired by Yu et al. (2020), we utilize ‘‘gradient surgery’’ to alleviate interference between different types of energy during energy preference optimization. More specifically, we have $\mathcal{E}(\cdot) = \sum_{v=1}^V w_v \mathcal{E}_v(\cdot)$, where V is the number of types of energy, and w_v is a constant weight for the v -th kind of energy. For each type of energy $\mathcal{E}_v(\cdot)$, we compute its corresponding energy preference gradient $\nabla_{\theta} L_v$ as Eq. (8), and then alter the gradient by projecting it onto the normal

plane of the other gradients (in a random order) if they have conflicts. This process works as follows:

$$\nabla_{\theta} L_v \leftarrow \nabla_{\theta} L_v - \frac{\min(\nabla_{\theta} L_v^{\top} \nabla_{\theta} L_u, 0)}{\|\nabla_{\theta} L_u\|^2} \nabla_{\theta} L_u, \quad (9)$$

where $v \in \{1, \dots, V\}$ and $u = \text{Shuffle}(1, \dots, V)$.

The complete direct energy-based preference optimization process can be summarized as Algorithm 1.

4 Experiments

4.1 Experimental Setup

Dataset Curation. To pre-train the diffusion model for antibody generation, we use the Structural Antibody Database (SAbDab, Dunbar et al., 2014) as the dataset. As suggested by Kong et al. (2023a), we collect antigen-antibody complexes renumbered under the IMGT (Lefranc et al., 2003) scheme with legal heavy chain, light chain, and protein antigen. We discarded the duplicate data with same CDR-L3 and CDR-H3. The remaining complexes are used to cluster via MMseqs2 (Steinegger & Söding, 2017) with 40% sequence similarity as the threshold based on the CDR-H3 sequence of each complex. We then select cluster that does not contain complexes in RAbD benchmark (Adolf-Bryfogle et al., 2018). We partition the complexes into training set and validation set at a ratio of 9:1. The validation set consists of complexes in the cluster that only contain one complex. We select 55 legal complexes from RAbD benchmark as the test set. The numbers of complexes are 1786 for training and 193 for validation.

For the data used in ABDPO fine-tuning, we first randomly sample 10,112 samples for each antigen-antibody complex in the test set using the aforementioned pre-trained diffusion model. Then, we use pyRosetta (Chaudhury et al., 2010) to apply the side chain packing and energy scoring (with default weights in Alford et al. (2017)) for these samples.

Preference Definition. To apply ABDPO, we need to build the preference dataset and construct the “winning” and “losing” pair $(\mathcal{R}_w^0, \mathcal{R}_l^0)$. We determine the preference according to three energies: CDR E_{total} for rationality; CDR-Ag E_{nonRep} and CDR-Ag E_{Rep} for functionality. Specifically, **(1)** CDR E_{total} is the total energy of the residues within the designed CDR, which is usually dominated by the repulsion risen from the massive structural clashes caused by the irrational relative position, and is used to represent the overall rationality of the corresponding residue; **(2)** CDR-Ag E_{nonRep} is the sum of the interaction energies except repulsion between the designed CDR residue and all antigen residues, exhibits attraction generally; and **(3)** CDR-Ag E_{Rep} is the repulsion energy between the design CDR residue and all antigen residues. For each of the three energies, the smaller is better and is assigned as “winning”. CDR-Ag E_{nonRep} and CDR-Ag E_{Rep} together constitute the interaction energy between the designed CDR residue and the target antigen, representing the functionality of the cor-

Table 1. Summary of CDR E_{total} and CDR-Ag ΔG (kcal/mol) of reference antibodies and antibodies designed by our model and baselines. (\downarrow) / (\uparrow) denotes a smaller / larger number is better.

Methods	CDR E_{total} (\downarrow)		CDR-Ag ΔG (\downarrow)		Success Rate (\uparrow)
	Avg.	Med.	Avg.	Med.	
Reference	4.52	-1.33	-13.72	-14.54	100%
HERN	7594.94	7825.92	1159.34	4.12	0%
MEAN	3113.7	2583.48	114.98	-0.92	0%
dyMEAN	15025.67	7426.4	2391	213.77	0%
dyMEAN*	3234.3	1690.91	1619.24	177.08	0%
DiffAb	211.00	155.77	9.54	-1.97	14.55%
ABDPO	162.75	124.62	-4.85	-5.24	27.27%

responding residue. We propose this decomposition due to the value of repulsion energy is usually several orders of magnitude larger than the other energies. We also conduct a more detailed calculation of the two functionality-associated energies in a more fine-grained way. Details can be found in Appendix B.

Baselines. We compare our model with various representative antibody sequence-structure co-design baselines. **HERN** (Jin et al., 2022a) designs sequences of antibodies autoregressively with iterative refinement of structures; **MEAN** (Kong et al., 2023a) generates sequences and structures of antibodies via a progress full-shot scheme; **dyMEAN** (Kong et al., 2023b) designs antibodies sequences and structures with full-atom modeling; **DiffAb** (Luo et al., 2022) models antibody distributions with a diffusion model that considers the amino acid type, C_{α} positions and side-chain orientations, which is a more rigorous *generative* model than the above baselines. The side-chain atoms are packed by pyRosetta. For **dyMEAN** which directly generates side-chain atoms, we use its generated side chains, and also implement a method that only uses its generated backbones and packs the side-chain atoms by pyRosetta, which is denoted as **dyMEAN***.

Evaluation. We generally utilize the energies introduced in the aforementioned preference definition to evaluate the designed antibodies from the perspectives of **rationality** and **functionality**, but at an instance level. Specifically, **(1)** the CDR E_{total} of the whole designed CDR is utilized to evaluate the rationality by aggregating all residues within the CDR; **(2)** CDR-Ag ΔG denotes the difference in total energy between the bound state and the unbound state of the CDR and antigen, which is calculated to evaluate the functionality. All methods are able to generate multiple antibodies for a specific antigen (a randomized version MEAN, rand-MEAN, is used here). We employ each method to design 2,528 antibodies, then rank the designs for each antigen using a uniform strategy (see Appendix D.3). We calculate the highest ranked design’s metrics for each antigen and report the mean and median metrics across all 55 antigens. We further report the percentage of antibodies which pass certain criteria as Success Rate (CDR $E_{\text{total}} < 65.90$

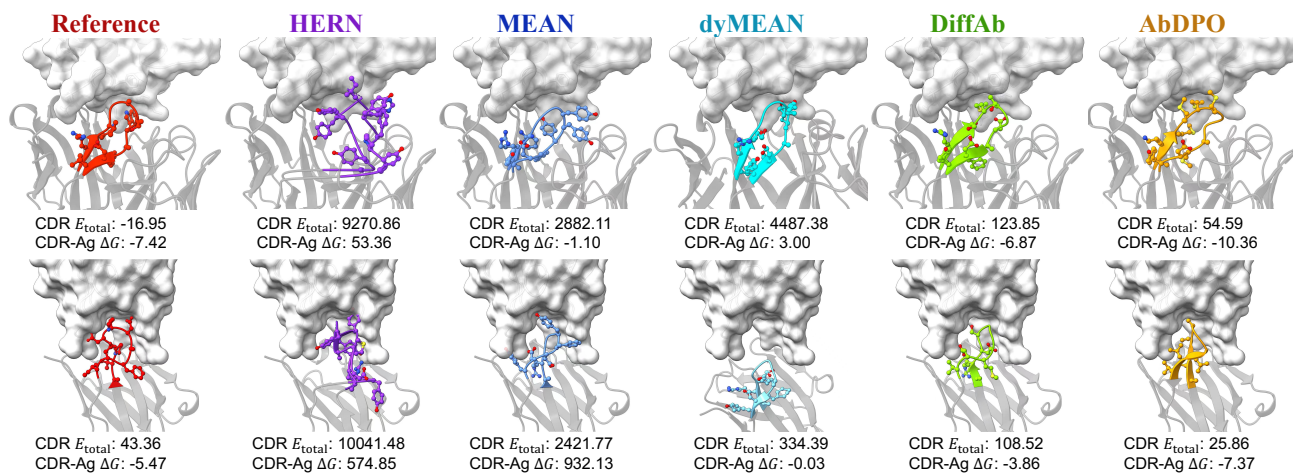


Figure 3. Visualization of reference antibodies in RAbD and antibodies designed by HERN, MEAN, dyMEAN, DiffAb, and ABDPO given specific antigens (PDB ID: 5mes (top) and 1iqd (bottom)). The unit of energy annotated is kcal/mol and omitted here for brevity.

kcal/mol and $CDR-Ag \Delta G < -0.82$ kcal/mol) to comprehensively evaluate the rationality and functionality. This metric is necessitated by the practical requirements of drug design, which mandate that the synthesized antibodies not only resemble rational structures, but also sustain high binding affinity simultaneously. The thresholds for $CDR E_{total}$ and $CDR-Ag \Delta G$ are computed as the 80-th percentile of antibodies in the training set.

4.2 Main Results

We report the evaluation metrics in Tab. 1. As the results show, ABDPO performs better than the other antibody sequence-structure co-design methods in all metrics. This demonstrates the effectiveness and superiority of ABDPO in terms of both rationality and functionality. We have also provided the full evaluation results in Appendix E.

It is observed that HERN, MEAN, and dyMEAN cannot design rational antibodies. Structural clashes in the generated antibodies are observed in these methods, and correspondingly, the $CDR E_{total}$ is high. The relative spatial relationship between the antigen and a high-quality antibody is also subtle. A too short distance between the antigen and antibody causes strong repulsion and leads a sharp increase in $CDR-Ag \Delta G$. On the contrary, a too long distance between the antigen and antibody means there is no interaction between them, in which case ΔG is approximately zero. These methods tend towards the former situation in terms of antigen-antibody relationship. By contrast, the results of DiffAb are much better and we think the reason are two fold: (a) DiffAb explicitly models the orientations of amino acids, which may help avoid generating structures with clashes caused by side chains; (b) DiffAb is a rigorous *generative model* and thus the diversity is guaranteed in theory, while other methods are not and in practice we have observed that the diversity of these methods is indeed inferior, which means the variance of the quality of the designed CDRs is low. Therefore, considering the top-1 ranked design, DiffAb

exhibits a higher probability of performing better than the other baselines. Compared with DiffAb, ABDPO has effectively reduced $CDR E_{total}$, which indicates fewer clashes, and also lowers $CDR-Ag \Delta G$ by a large margin, which indicates stronger binding affinity. Notably, the Success Rate of ABDPO achieves 40.00%.

We also visualize two cases (PDB ID: 5mes and 1iqd) in Fig. 3. It is shown that ABDPO can design CDRs with both fewer clashes and proper relative spatial positions towards the antigens, while other methods perform unsatisfactorily. We conduct an additional experiment where we compute the energy of synthetic antibodies whose structures are further optimized by Rosetta as the preference. In this experiment, the antibodies designed by ABDPO are on par with real-world antibodies. Refer to Appendix E.3 for related details.

4.3 Ablation Studies

Our approach is composed of three main novel designs, including residue-level direct energy-based preference optimization, energy decomposition and conflict mitigation by gradient surgery. Thus we perform comprehensive ablation studies to verify our hypothesis on the effects of each respective design component. Here we take the experiment on an antigen (PDB ID: 1a14) as an example. More cases of the ablation studies can be found in Appendix F.

Effects of Residue-level Energy Preference Optimization.

We hypothesize that residue-level DPO leads to more explicit and intuitive gradients that can promote effectiveness and efficiency compared with the vanilla DPO (Wallace et al., 2023) as the analysis in Sec. 3.2. To validate this, we compare ABDPO with its counterpart with the CDR-level preference instead of residue-level. As Fig. 4 shows, regarding the counterpart (blue dotted line), the changes in all metrics are not obvious, while almost all metrics rapidly converge to an ideal state in ABDPO (red line). This demonstrated the effects of residue-level energy preference in improving the optimization efficiency.

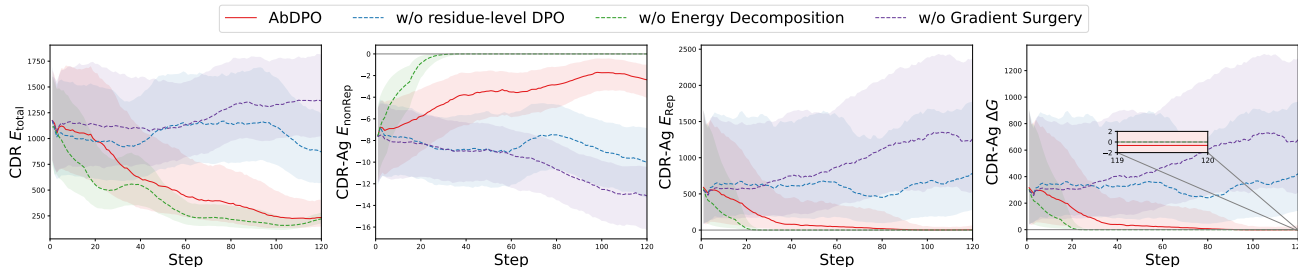


Figure 4. Changes of median CDR E_{total} , CDR-Ag E_{nonRep} , CDR-Ag E_{Rep} , and CDR-Ag ΔG (kcal/mol) over optimization steps, shaded to indicate interquartile range (from 25-th percentile to 75-th percentile).

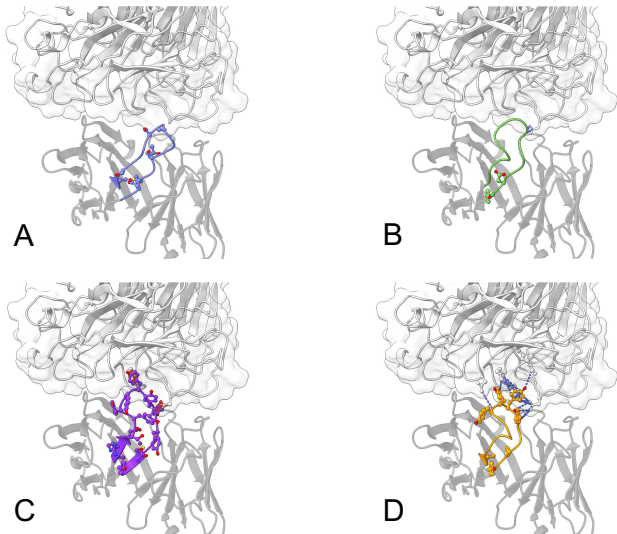


Figure 5. Typical generated samples from different preferences. **A:** using preference solely relies on CDR E_{total} , the generated antibody tends to have fewer side chains and is far from the antigen. **B:** using preference relies on CDR E_{total} and ΔG , the outcome is similar to the previous. **C:** using preference relies on CDR E_{total} and CDR-Ag E_{nonRep} , the outcome tends to have large side chains and is overly close to the antigen. **D:** using the preference in ABDPO, the generated antibody eliminates the clashes while maintaining the interactions (blue dashed lines) between the antigen.

Effects of Energy Decomposition. In generated antibodies, the huge repulsion caused by clashes accounts for the majority of the total energy. This prevents us from using the ΔG as an optimization objective directly as the model is allowed to minimize repulsion by keeping antibodies away from antigens, quickly reducing the total energy. To verify this, we compared ABDPO with a version that does not implement energy decomposition in which E_{Rep} and E_{nonRep} are aggregated into ΔG . As shown in Fig. 4, without energy decomposition (green dashed line), both E_{Rep} and E_{nonRep} quickly diminish to 0, indicating that there is no interaction between the generated antibodies and antigens. Conversely, ABDPO (red line) can optimize E_{Rep} to 0 while maintaining E_{nonRep} , which means that it preserves the interaction between antibodies and antigens while eliminating clashes. In practice, we experimented with several energy combinations, and Fig. 5 displays the typical generated sample from

Table 2. Comparison of ABDPO and supervised fine-tuning (SFT).

Methods	CDR E_{total} (\downarrow)		CDR-Ag ΔG (\downarrow)	
	Avg.	Med.	Avg.	Med.
Reference	62.28	62.28	-4.72	-4.72
DiffAb	288.10	289.81	0.84	-1.03
DiffAb _{SFT}	274.01	281.47	-2.72	-2.65
ABDPO	88.15	85.13	-2.97	-2.66

each combination, illustrating the trends of the results with different energy preference settings.

Effects of Gradient Surgery. To show the effectiveness of gradient surgery in mitigating the conflicts when optimizing multiple types of energy, we compare ABDPO and its counterpart without gradient surgery. As Fig. 4 shows, the counterpart can only slightly optimize CDR-Ag E_{nonRep} but incurs strong repulsion (i.e., E_{Rep}), learning to irrational structures. ABDPO (red line) can converge to a state where CDR E_{total} and CDR-Ag E_{Rep} achieve a conspicuously low point, suggesting the generated sequences and structures are stable, and CDR-Ag E_{nonRep} is still significantly less than zero, showing that considerable binding affinity is kept.

Comparison with Supervised Fine-tuning. Supervised Fine-tuning (SFT) can be an alternative way of generating antibodies with lower energy. For SFT, we first select top 10% high-quality complexes from ABDPO training data on an antigen (PDB ID: 1a14). We fine-tune the diffusion model under the same settings as ABDPO. Results in Tab. 2 show that SFT only marginally surpasses the pre-trained diffusion model, and ABDPO performs significantly superior to SFT. We attribute the performance of ABDPO to the preference optimization scheme and the fine-grained residue-level energy rather than the entire CDR.

5 Conclusions

In this work, we rethink antibody sequence-structure co-design through the lens of energy and proposed ABDPO for designing antibodies considering both rationality and functionality. The introduction of direct energy-based preference optimization along with energy decomposition and conflict mitigation by gradient surgery shows promising results in generating antibodies with low energy and high binding affinity. Limitations and future work are discussed

in Appendix G.

Impact Statements

Our work on antibody design can be used in developing potent therapeutic antibodies and accelerate the research process of drug discovery. Our method may be adapted to other scenarios of computer-aided design, such as small molecule design, material design, and chip design. It is also needed to ensure the responsible use of our method and refrain from using it for harmful purposes.

References

- Adolf-Bryfogle, J., Kalyuzhnyi, O., Kubitz, M., Weitzner, B. D., Hu, X., Adachi, Y., Schief, W. R., and Dunbrack Jr, R. L. Rosettaantibodydesign (rabd): A general framework for computational antibody design. *PLoS computational biology*, 14(4):e1006112, 2018.
- Akbar, R., Robert, P. A., Pavlović, M., Jeliazkov, J. R., Snapkov, I., Slabodkin, A., Weber, C. R., Scheffer, L., Miho, E., Haff, I. H., Haug, D. T. T., Lund-Johansen, F., Safonova, Y., Sandve, G. K., and Greiff, V. A compact vocabulary of paratope-epitope interactions enables predictability of antibody-antigen binding. *Cell Reports*, 34(11):108856, 2021. ISSN 2211-1247. doi: <https://doi.org/10.1016/j.celrep.2021.108856>. URL <https://www.sciencedirect.com/science/article/pii/S2211124721001704>.
- Akbar, R., Robert, P. A., Weber, C. R., Widrich, M., Frank, R., Pavlović, M., Scheffer, L., Chernigovskaya, M., Snapkov, I., Slabodkin, A., et al. In silico proof of principle of machine learning-based antibody design at unconstrained scale. In *MABs*, volume 14, pp. 2031482. Taylor & Francis, 2022.
- Alford, R. F., Leaver-Fay, A., Jeliazkov, J. R., O’Meara, M. J., DiMaio, F. P., Park, H., Shapovalov, M. V., Renfrew, P. D., Mulligan, V. K., Kappel, K., Labonte, J. W., Pacella, M. S., Bonneau, R., Bradley, P., Dunbrack, R. L. J., Das, R., Baker, D., Kuhlman, B., Kortemme, T., and Gray, J. J. The rosetta all-atom energy function for macromolecular modeling and design. *Journal of Chemical Theory and Computation*, 13(6):3031–3048, 2017. doi: 10.1021/acs.jctc.7b00125. URL <https://doi.org/10.1021/acs.jctc.7b00125>. PMID: 28430426.
- Alley, E. C., Khimulya, G., Biswas, S., AlQuraishi, M., and Church, G. M. Unified rational protein engineering with sequence-based deep representation learning. *Nature methods*, 16(12):1315–1322, 2019.
- Anonymous. Proximal preference optimization for diffusion models, 2023. URL <https://openreview.net/forum?id=u8fg8acFsT>.
- Black, K., Janner, M., Du, Y., Kostrikov, I., and Levine, S. Training diffusion models with reinforcement learning. *arXiv preprint arXiv:2305.13301*, 2023.
- Bradley, R. A. and Terry, M. E. Rank analysis of incomplete block designs: I. the method of paired comparisons. *Biometrika*, 39(3/4):324–345, 1952.
- Chaudhury, S., Lyskov, S., and Gray, J. J. PyRosetta: a script-based interface for implementing molecular modeling algorithms using Rosetta. *Bioinformatics*, 26(5):689–691, 01 2010. ISSN 1367-4803. doi: 10.1093/bioinformatics/btq007. URL <https://doi.org/10.1093/bioinformatics/btq007>.
- Chen, Z., Deng, Y., Yuan, H., Ji, K., and Gu, Q. Self-play fine-tuning converts weak language models to strong language models. *arXiv preprint arXiv:2401.01335*, 2024.
- Crooks, G. E., Hon, G., Chandonia, J.-M., and Brenner, S. E. Weblogo: a sequence logo generator. *Genome research*, 14(6):1188–1190, 2004.
- Dong, J., Zost, S. J., Greaney, A. J., Starr, T. N., Dingens, A. S., Chen, E. C., Chen, R. E., Case, J. B., Sutton, R. E., Gilchuk, P., et al. Genetic and structural basis for sars-cov-2 variant neutralization by a two-antibody cocktail. *Nature microbiology*, 6(10):1233–1244, 2021.
- Dunbar, J., Krawczyk, K., Leem, J., Baker, T., Fuchs, A., Georges, G., Shi, J., and Deane, C. M. Sabdab: the structural antibody database. *Nucleic acids research*, 42(D1):D1140–D1146, 2014.
- Eastman, P., Swails, J., Chodera, J. D., McGibbon, R. T., Zhao, Y., Beauchamp, K. A., Wang, L.-P., Simmonett, A. C., Harrigan, M. P., Stern, C. D., et al. Openmm 7: Rapid development of high performance algorithms for molecular dynamics. *PLoS computational biology*, 13(7):e1005659, 2017.
- Ewert, S., Honegger, A., and Plückthun, A. Stability improvement of antibodies for extracellular and intracellular applications: Cdr grafting to stable frameworks and structure-based framework engineering. *Methods*, 34(2):184–199, 2004. ISSN 1046-2023. doi: <https://doi.org/10.1016/j.jymeth.2004.04.007>. URL <https://www.sciencedirect.com/science/article/pii/S1046202304000738>. Intrabodies.
- Fan, Y., Watkins, O., Du, Y., Liu, H., Ryu, M., Boutilier, C., Abbeel, P., Ghavamzadeh, M., Lee, K., and Lee, K. Reinforcement learning for fine-tuning text-to-image diffusion models. In *Thirty-seventh Conference on Neural Information Processing Systems*, 2023. URL <https://openreview.net/forum?id=80TepXzeh>.

- Ferruz, N., Schmidt, S., and Höcker, B. Protgpt2 is a deep unsupervised language model for protein design. *Nature communications*, 13(1):4348, 2022.
- Gallier, J. and Xu, D. Computing exponentials of skew-symmetric matrices and logarithms of orthogonal matrices. *International Journal of Robotics and Automation*, 18(1):10–20, 2003.
- Gao, K., Wu, L., Zhu, J., Peng, T., Xia, Y., He, L., Xie, S., Qin, T., Liu, H., He, K., et al. Pre-training antibody language models for antigen-specific computational antibody design. In *Proceedings of the 29th ACM SIGKDD Conference on Knowledge Discovery and Data Mining*, pp. 506–517, 2023.
- Ho, J., Jain, A., and Abbeel, P. Denoising diffusion probabilistic models. In Larochelle, H., Ranzato, M., Hadsell, R., Balcan, M., and Lin, H. (eds.), *Advances in Neural Information Processing Systems*, volume 33, pp. 6840–6851. Curran Associates, Inc., 2020. URL https://proceedings.neurips.cc/paper_files/paper/2020/file/4c5bcfec8584af0d967f1ab10179ca4b-Paper.pdf.
- Jin, W., Barzilay, R., and Jaakkola, T. Antibody-antigen docking and design via hierarchical structure refinement. In *International Conference on Machine Learning*, pp. 10217–10227. PMLR, 2022a.
- Jin, W., Wohlwend, J., Barzilay, R., and Jaakkola, T. S. Iterative refinement graph neural network for antibody sequence-structure co-design. In *International Conference on Learning Representations*, 2022b. URL https://openreview.net/forum?id=LI2bhrE_2A.
- Jing, B., Eismann, S., Suriana, P., Townshend, R. J. L., and Dror, R. Learning from protein structure with geometric vector perceptrons. In *International Conference on Learning Representations*, 2021. URL <https://openreview.net/forum?id=1YLJDvSx6J4>.
- Jones, P. T., Dear, P. H., Foote, J., Neuberger, M. S., and Winter, G. Replacing the complementarity-determining regions in a human antibody with those from a mouse. *Nature*, 321(6069):522–525, 1986.
- Jumper, J., Evans, R., Pritzel, A., Green, T., Figurnov, M., Ronneberger, O., Tunyasuvunakool, K., Bates, R., Židek, A., Potapenko, A., et al. Highly accurate protein structure prediction with alphafold. *Nature*, 596(7873):583–589, 2021.
- Katoh, K. and Standley, D. M. Mafft multiple sequence alignment software version 7: improvements in performance and usability. *Molecular biology and evolution*, 30(4):772–780, 2013.
- Kingma, D. P. and Ba, J. Adam: A method for stochastic optimization. *arXiv preprint arXiv:1412.6980*, 2014.
- Kofinas, M., Nagaraja, N. S., and Gavves, E. Roto-translated local coordinate frames for interacting dynamical systems. In Beygelzimer, A., Dauphin, Y., Liang, P., and Vaughan, J. W. (eds.), *Advances in Neural Information Processing Systems*, 2021. URL <https://openreview.net/forum?id=c3RKZas9am>.
- Kong, X., Huang, W., and Liu, Y. Conditional antibody design as 3d equivariant graph translation. In *The Eleventh International Conference on Learning Representations*, 2023a. URL <https://openreview.net/forum?id=LFHFQbjxIiP>.
- Kong, X., Huang, W., and Liu, Y. End-to-end full-atom antibody design. In Krause, A., Brunskill, E., Cho, K., Engelhardt, B., Sabato, S., and Scarlett, J. (eds.), *Proceedings of the 40th International Conference on Machine Learning*, volume 202 of *Proceedings of Machine Learning Research*, pp. 17409–17429. PMLR, 23–29 Jul 2023b.
- Lapidoth, G. D., Baran, D., Pszolla, G. M., Norn, C., Alon, A., Tyka, M. D., and Fleishman, S. J. Abdesign: A n algorithm for combinatorial backbone design guided by natural conformations and sequences. *Proteins: Structure, Function, and Bioinformatics*, 83(8):1385–1406, 2015.
- Leach, A., Schmon, S. M., Degiacomi, M. T., and Willcocks, C. G. Denoising diffusion probabilistic models on so (3) for rotational alignment. In *ICLR 2022 Workshop on Geometrical and Topological Representation Learning*, 2022.
- Lee, H., Phatale, S., Mansoor, H., Lu, K., Mesnard, T., Bishop, C., Carbune, V., and Rastogi, A. Rlaif: Scaling reinforcement learning from human feedback with ai feedback. *arXiv preprint arXiv:2309.00267*, 2023.
- Lefranc, M.-P., Pommié, C., Ruiz, M., Giudicelli, V., Foulquier, E., Truong, L., Thouvenin-Contet, V., and Lefranc, G. Imgt unique numbering for immunoglobulin and t cell receptor variable domains and ig superfamily v-like domains. *Developmental & Comparative Immunology*, 27(1):55–77, 2003.
- Liu, G., Zeng, H., Mueller, J., Carter, B., Wang, Z., Schilz, J., Horny, G., Birnbaum, M. E., Ewert, S., and Gifford, D. K. Antibody complementarity determining region design using high-capacity machine learning. *Bioinformatics*, 36(7):2126–2133, 2020.
- Luo, S., Su, Y., Peng, X., Wang, S., Peng, J., and Ma, J. Antigen-specific antibody design and optimization with diffusion-based generative models for protein structures. In Oh, A. H., Agarwal, A., Belgrave, D., and Cho,

- K. (eds.), *Advances in Neural Information Processing Systems*, 2022. URL <https://openreview.net/forum?id=jSorGn2Tjg>.
- Martinkus, K., Ludwiczak, J., LIANG, W.-C., Lafrance-Vanasse, J., Hotzel, I., Rajpal, A., Wu, Y., Cho, K., Bonneau, R., Gligorijevic, V., and Loukas, A. Abdifuser: full-atom generation of in-vitro functioning antibodies. In *Thirty-seventh Conference on Neural Information Processing Systems*, 2023. URL <https://openreview.net/forum?id=7GyYpomkEa>.
- Miyazawa, S. and Jernigan, R. L. Estimation of effective interresidue contact energies from protein crystal structures: quasi-chemical approximation. *Macromolecules*, 18(3):534–552, 1985.
- Murphy, K. and Weaver, C. *Janeway’s immunobiology*. Garland science, 2016.
- Ouyang, L., Wu, J., Jiang, X., Almeida, D., Wainwright, C., Mishkin, P., Zhang, C., Agarwal, S., Slama, K., Gray, A., Schulman, J., Hilton, J., Kelton, F., Miller, L., Simens, M., Askell, A., Welinder, P., Christiano, P., Leike, J., and Lowe, R. Training language models to follow instructions with human feedback. In Oh, A. H., Agarwal, A., Belgrave, D., and Cho, K. (eds.), *Advances in Neural Information Processing Systems*, 2022. URL <https://openreview.net/forum?id=TG8KACxEON>.
- Rafailov, R., Sharma, A., Mitchell, E., Manning, C. D., Ermon, S., and Finn, C. Direct preference optimization: Your language model is secretly a reward model. In *Thirty-seventh Conference on Neural Information Processing Systems*, 2023. URL <https://arxiv.org/abs/2305.18290>.
- Saka, K., Kakuzaki, T., Metsugi, S., Kashiwagi, D., Yoshida, K., Wada, M., Tsunoda, H., and Teramoto, R. Antibody design using lstm based deep generative model from phage display library for affinity maturation. *Scientific reports*, 11(1):5852, 2021.
- Steinegger, M. and Söding, J. Mmseqs2 enables sensitive protein sequence searching for the analysis of massive data sets. *Nature biotechnology*, 35(11):1026–1028, 2017.
- Victoria, G. D. and Nussenzweig, M. C. Germinal centers. *Annual review of immunology*, 30:429–457, 2012.
- Wallace, B., Dang, M., Rafailov, R., Zhou, L., Lou, A., Purushwalkam, S., Ermon, S., Xiong, C., Joty, S., and Naik, N. Diffusion model alignment using direct preference optimization. *arXiv preprint arXiv:2311.12908*, 2023.
- Warszawski, S., Borenstein Katz, A., Lipsh, R., Khmelnitsky, L., Ben Nissan, G., Javitt, G., Dym, O., Unger, T., Knop, O., Albeck, S., et al. Optimizing antibody affinity and stability by the automated design of the variable light-heavy chain interfaces. *PLoS computational biology*, 15(8):e1007207, 2019.
- Wu, F. and Li, S. Z. A hierarchical training paradigm for antibody structure-sequence co-design. In *Thirty-seventh Conference on Neural Information Processing Systems*, 2023. URL <https://openreview.net/forum?id=hV52oj0Sik>.
- Xu, J. L. and Davis, M. M. Diversity in the cdr3 region of vh is sufficient for most antibody specificities. *Immunity*, 13(1):37–45, 2000. ISSN 1074-7613. doi: [https://doi.org/10.1016/S1074-7613\(00\)00006-6](https://doi.org/10.1016/S1074-7613(00)00006-6). URL <https://www.sciencedirect.com/science/article/pii/S1074761300000066>.
- Yim, J., Trippe, B. L., De Bortoli, V., Mathieu, E., Doucet, A., Barzilay, R., and Jaakkola, T. SE(3) diffusion model with application to protein backbone generation. In Krause, A., Brunskill, E., Cho, K., Engelhardt, B., Sabato, S., and Scarlett, J. (eds.), *Proceedings of the 40th International Conference on Machine Learning*, volume 202 of *Proceedings of Machine Learning Research*, pp. 40001–40039. PMLR, 23–29 Jul 2023.
- Yu, T., Kumar, S., Gupta, A., Levine, S., Hausman, K., and Finn, C. Gradient surgery for multi-task learning. *Advances in Neural Information Processing Systems*, 33: 5824–5836, 2020.
- Zheng, Z., Deng, Y., Xue, D., Zhou, Y., YE, F., and Gu, Q. Structure-informed language models are protein designers. In *International Conference on Machine Learning*, 2023.
- Zhou, X., Wang, L., and Zhou, Y. Stabilizing policy gradients for stochastic differential equations via consistency with perturbation process. *arXiv preprint arXiv:2403.04154*, 2024.

A Motivation for Choosing Energy as Evaluation

There are many limitations in using AAR and RMSD as the main evaluation metrics in AI-based antibody design. Antibody design is a typical function-oriented protein design task, necessitating a more fine-grained measure of discrepancy compared to general protein design tasks. Especially when the part of the antibody to be designed and evaluated, CDR-H3, is usually shorter, more precise evaluation becomes particularly important.

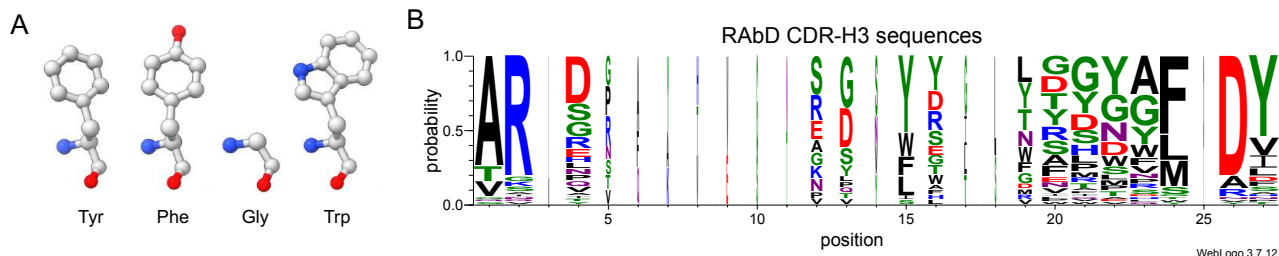


Figure 6. **A:** Tyr (Y) and Phe (F) differ by only one oxygen atom. In contrast, there is a substantial difference between Gly (G) and Trp (W). Gly lacks a side chain, whereas Trp possesses the largest side chain of all amino acids. **B:** the visualization of the frequency of occurrence of each amino acid at various positions in RAbD CDR-H3 sequences. The sequences are initially aligned using MAFFT (Katoh & Standley, 2013) and subsequently visualized with WebLogo (Crooks et al., 2004). The width of each column corresponds to the frequency of occurrence at that position.

For AAR, there are two main limitations in measuring the similarity between the generated sequence and the reference sequence. The first limitation is located in measuring the difference in different incorrect recovery. Among the 20 common amino acids, some have high similarity between them, such as Tyr and Phe, while others have significant differences, such as Gly and Trp (Fig. 6A). When an amino acid in CDR is erroneously recovered to different amino acids, their impact will also vary. However, AAR does not differentiate between these different types of errors, only identifying them as “incorrect”. A further, more serious issue is that AAR is easily hacked. Although the CDR region is often considered hypervariable, a mild conservatism in sequence still exists (Fig. 6B), which allows the model to obtain satisfactory AAR using a simple but incorrect way - directly generating the amino acids with the highest probability of occurrence at each position, while ignoring the condition of the given antigen which is extremely harmful for the specificity of antibodies. We made a simple attempt by simply counting the amino acids with the highest frequency of occurrence at various positions in all samples in SAbDab, and then composing them into a CDR-H3 sequence, which looks roughly like “ARD + rand(Y, G)* + FDY”, achieving an AAR of **38.77%** on the RAbD dataset.

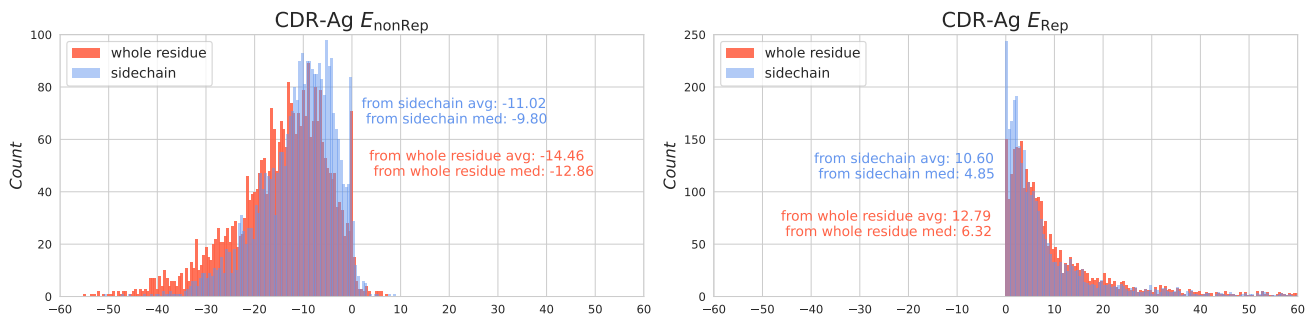


Figure 7. The distribution of CDR-Ag E_{nonRep} (left) and CDR-Ag E_{Rep} (right) formed by the whole CDR atoms (colored in red) and solely by CDR side-chain atoms (colored in blue) among SAbDab dataset.

While RMSD fails in measuring the discrepancies on side-chain atoms. In general, the calculation of RMSD focus on the alpha carbon atom or the four backbone atoms due to their stable existence in any type of amino acids and thus ignore the side-chain atoms. However, side-chain atoms in CDR region are extremely important as they contribute most of the interactions between the CDR and the antigen. Our analyses on SAbDab dataset also prove the importance of the side chain in CDR-Antigen interaction in terms of energy. As shown in Fig. 7, the distribution of energies formed by the whole residues in CDR is colored in red while the distribution of energies formed only by side-chain atoms of CDR is colored in blue. The interaction energy formed by side-chain atoms accounts for the vast majority of the total interaction energy in

both types of energy.

An additional issue that involves both AAR and RMSD is that, when one of the sequences/structures of CDR is not the same as the reference CDR, we should not expect the other one to be consistent with the reference CDR.

The above reasons have led us to abandon AAR and RMSD as learning objectives and evaluation metrics, and instead use energy as our goal. Energy can simultaneously consider the relationship between structure and sequence, distinguish different generation results in more detail, and importantly, reflect the rationality and functionality of antibodies in a more fundamental way. Despite the various shortcomings of AAR and RMSD, we have demonstrated that the antibodies generated by ABDPO achieve lower AAR and comparable RMSD compared to those generated by other methods (see Tab. 3). However, in practice, ABDPO-generated antibodies exhibit distinct binding patterns to antigens, differing from reference antibodies, and demonstrate significantly better energy performance than those produced by other methods. This further highlights the inadequacies of using AAR and RMSD as evaluation metrics in antibody design tasks, exposing their vulnerability to being “hacked”.

Table 3. AAR and RMSD evaluation results for baselines and ABDPO are presented across three tables in a left-right order: (1) using default sampling settings from their paper and codebase; (2) comparing ranked top-1 antibodies; (3) comparing all 2,528 antibodies aforementioned in Sec. 4.1. We use ranked top-1 antibodies designed by ABDPO for comparison in the first two tables.

Method	AAR	RMSD	Method	AAR	RMSD	Method	AAR	RMSD
HERN	33.17%	9.86	HERN	22.35%	9.79	HERN	24.79%	9.78
MEAN	33.47%	1.82	MEAN	35.95%	1.92	MEAN	36.24%	1.97
dyMEAN	40.95%	7.24	dyMEAN	41.95%	7.31	dyMEAN	41.28%	7.31
DiffAb	36.42%	2.34	DiffAb	36.77%	2.14	DiffAb	36.52%	2.47
ABDPO	26.46%	2.48	ABDPO	26.46%	2.48	ABDPO	25.95%	2.77

B Energy Calculation

In ABDPO, we conduct the calculation on CDR E_{total} at residue level, and a more fine-grained calculation on the two functionality-associated energies at the sub-residue level.

We denote the residue with the index i in the antibody-antigen complex as A_i , then A_i^{sc} and A_i^{bb} represent the **side chain** and **backbone** of the residue respectively.

For the energies in the proposed preference, we describe the function for energies of a Single residue as ES, and ES_{total} is the sum of all types of energy with the default weight in REF15 (Alford et al., 2017). The function for interaction energies between Paired residues is described as EP, which consists of six different energy types: EP_{hbond} , EP_{att} , EP_{rep} , EP_{sol} , EP_{elec} , and EP_{lk} .

Following the settings previously mentioned in Sec. 3.1 that the indices of residues within the CDR-H3 range from $l + 1$ to $l + m$, and the indices of residues within the antigen range from $g + 1$ to $g + n$. Then, for the CDR residue with the index j , the three types of energy are defined as:

$$\text{CDR } E_{\text{total}}^j = \text{ES}_{\text{total}}(A_j), \tag{10}$$

$$\text{CDR-Ag } E_{\text{nonRep}}^j = \sum_{i=g+1}^{g+n} \sum_{e \in \{\text{hbond, att, sol, elec, lk}\}} \left(EP_e(A_j^{sc}, A_i^{sc}) + EP_e(A_j^{sc}, A_i^{bb}) \right), \tag{11}$$

$$\text{CDR-Ag } E_{\text{Rep}}^j = \sum_{i=g+1}^{g+n} \left(EP_{\text{rep}}(A_j^{sc}, A_i^{sc}) + EP_{\text{rep}}(A_j^{sc}, A_i^{bb}) + 2 \times EP_{\text{rep}}(A_j^{bb}, A_i^{sc}) + 2 \times EP_{\text{rep}}(A_j^{bb}, A_i^{bb}) \right). \tag{12}$$

It can be observed from Eqs. (11) and (12) that the two energies, namely CDR-Ag E_{nonRep} and CDR-Ag E_{Rep} , which collectively describe the interaction energy between CDR and the antigen, are computed at the level of side chain and backbone. CDR-Ag E_{nonRep} is only calculated on the interactions caused by the side-chain atoms in the CDR-H3 region, while CDR-Ag E_{Rep} assigns a greater cost to the repulsions caused by the backbone atoms in the CDR-H3 region. This modification is carried out according to the fact that the side-chain atoms contribute the vast majority of energy to the interaction between CDR-H3 and antigens (Fig. 7), and CDR-Ag E_{nonRep} exhibits a benefit in interactions, while CDR-Ag E_{Rep} could be regarded as cost.

The fine-grained calculation of CDR-Ag E_{nonRep} and CDR-Ag E_{Rep} is indispensable. Without the fine-grained calculation, the model tends to generate poly-G CDR-H3 sequences, such as “GGGGGGGGGG” for any given antigen and the rest of the antibody. The most likely reason for this is that G, Glycine, can maximize the reduction of clashes and gain satisfactory

CDR E_{total} and CDR-Ag E_{Rep} as it doesn't contain side chain and simultaneously form weak attraction to the antigen solely relying on its backbone atoms.

We emphasize that the two functionality-associated energies, CDR-Ag E_{nonRep} and CDR-Ag E_{Rep} are calculated exclusively at the sub-residue level when serving as the determination of preference in guiding the direct energy-based preference optimization process. However, when these energies are used as evaluation metrics, they are calculated at the residue level, in which the greater cost to the repulsions attributed to the backbone atoms is negated.

C Theoretical Justification

In this section, we show the detailed mathematical derivations of formulas in [Sec. 3.2](#). Although many of them are similar to [Rafailov et al. \(2023\)](#), we still present them in detail for the sake of completeness. Besides, we will also present the details of preference data generation.

First, we will show the derivation of the optimal solution of the KL-constrained reward-maximization objective, i.e., $\max_{p_\theta} \mathbb{E}_{\mathcal{R}^0 \sim p_\theta} [r(\mathcal{R}^0)] - \beta \mathbb{D}_{\text{KL}}(p_\theta(\mathcal{R}^0) \| p_{\text{ref}}(\mathcal{R}^0))$ as follows:

$$\begin{aligned} & \max_{p_\theta} \mathbb{E}_{\mathcal{R}^0 \sim p_\theta} [r(\mathcal{R}^0)] - \beta \mathbb{D}_{\text{KL}}(p_\theta(\mathcal{R}^0) \| p_{\text{ref}}(\mathcal{R}^0)) \\ &= \max_{p_\theta} \mathbb{E}_{\mathcal{R}^0 \sim p_\theta} \left[r(\mathcal{R}^0) - \beta \log \frac{p_\theta(\mathcal{R}^0)}{p_{\text{ref}}(\mathcal{R}^0)} \right] \\ &= \min_{p_\theta} \mathbb{E}_{\mathcal{R}^0 \sim p_\theta} \left[\log \frac{p_\theta(\mathcal{R}^0)}{p_{\text{ref}}(\mathcal{R}^0)} - \frac{1}{\beta} r(\mathcal{R}^0) \right] \\ &= \min_{p_\theta} \mathbb{E}_{\mathcal{R}^0 \sim p_\theta} \left[\log \frac{p_\theta(\mathcal{R}^0)}{\frac{1}{Z} p_{\text{ref}}(\mathcal{R}^0) \exp\left(\frac{1}{\beta} r(\mathcal{R}^0)\right)} - \log Z \right] \end{aligned}$$

where Z is the partition function that does not involve the model being trained, i.e., p_θ . And we can define

$$p^*(\mathcal{R}^0) := \frac{1}{Z} p_{\text{ref}}(\mathcal{R}^0) \exp\left(\frac{1}{\beta} r(\mathcal{R}^0)\right).$$

With this, we can now arrive at

$$\begin{aligned} & \min_{p_\theta} \mathbb{E}_{\mathcal{R}^0 \sim p_\theta} \left[\log \frac{p_\theta(\mathcal{R}^0)}{p^*(\mathcal{R}^0)} \right] - \log Z \\ &= \min_{p_\theta} \mathbb{E}_{\mathcal{R}^0 \sim p_\theta} [\mathbb{D}_{\text{KL}}(p_\theta \| p^*)] + Z \end{aligned}$$

Since Z does not depend on p_θ , we can directly drop it. According to Gibb's inequality that KL-divergence is minimized at 0 if and only if the two distributions are identical. Hence we arrive at the optimum as follows:

$$p_{\theta^*}(\mathcal{R}^0) = p^*(\mathcal{R}^0) = \frac{1}{Z} p_{\text{ref}}(\mathcal{R}^0) \exp\left(\frac{1}{\beta} r(\mathcal{R}^0)\right). \quad (13)$$

Then we will show that the objective that maximizes likelihood on preference data sampled from $p(\mathcal{R}_1^0 \succ \mathcal{R}_2^0) = \sigma(r(\mathcal{R}_1^0) - r(\mathcal{R}_2^0))$, which is exactly L_{DPO} , leads to the same optimal solution. For this, we need to express the pre-defined reward $r(\cdot)$ with the optimal policy p^* :

$$r(\mathcal{R}^0) = \beta \log \frac{p^*(\mathcal{R}^0)}{p_{\text{ref}}(\mathcal{R}^0)} + Z$$

The we plugin the expression of $r(\cdot)$ into $p(\mathcal{R}_1^0 \succ \mathcal{R}_2^0) = \sigma(r(\mathcal{R}_1^0) - r(\mathcal{R}_2^0))$ as follows:

$$\begin{aligned} p(\mathcal{R}_1^0 \succ \mathcal{R}_2^0) &= \sigma(r(\mathcal{R}_1^0) - r(\mathcal{R}_2^0)) \\ &= \sigma\left(\beta \log \frac{p^*(\mathcal{R}_1^0)}{p_{\text{ref}}(\mathcal{R}_1^0)} - \beta \log \frac{p^*(\mathcal{R}_2^0)}{p_{\text{ref}}(\mathcal{R}_2^0)}\right), \end{aligned}$$

where Z is canceled out. For brevity, we use the following notation for brevity:

$$p_\theta(\mathcal{R}_1^0 \succ \mathcal{R}_2^0) = \sigma\left(\beta \log \frac{p_\theta(\mathcal{R}_1^0)}{p_{\text{ref}}(\mathcal{R}_1^0)} - \beta \log \frac{p_\theta(\mathcal{R}_2^0)}{p_{\text{ref}}(\mathcal{R}_2^0)}\right).$$

With this, we have

$$\begin{aligned} \min_{p_\theta} L_{\text{DPO}} &= \min_{p_\theta} -\mathbb{E}_{\mathcal{R}_1^0, \mathcal{R}_2^0 \sim p(\mathcal{R}_1^0 \succ \mathcal{R}_2^0)} p_\theta(\mathcal{R}_1^0 \succ \mathcal{R}_2^0) \\ &= \max_{p_\theta} \mathbb{E}_{\mathcal{R}_1^0, \mathcal{R}_2^0 \sim p(\mathcal{R}_1^0 \succ \mathcal{R}_2^0)} p_\theta(\mathcal{R}_1^0 \succ \mathcal{R}_2^0) \\ &= \min_{p_\theta} \mathbb{D}_{\text{KL}}\left(p(\mathcal{R}_1^0 \succ \mathcal{R}_2^0) \parallel p_\theta(\mathcal{R}_1^0 \succ \mathcal{R}_2^0)\right) \end{aligned}$$

Again with Gibb’s inequality, we can easily identify that $p_\theta(\mathcal{R}_1^0 \succ \mathcal{R}_2^0) = p(\mathcal{R}_1^0 \succ \mathcal{R}_2^0)$ achieves the minimum. Thus $p^*(\mathcal{R}^0) = \frac{1}{Z} p_{\text{ref}}(\mathcal{R}^0) \exp\left(\frac{1}{\beta} r(\mathcal{R}^0)\right)$ is also the optimal solution of L_{DPO} .

In our case, antibodies with low energy are preferred. Thus we define reward as $r(\cdot) := -\mathcal{E}(\cdot)/\mathcal{T}$, where $\mathcal{E}(\cdot)$ is the energy function and \mathcal{T} is the temperature. In practice, we set $1/\mathcal{T}$ to a sufficiently large constant. The reason is that as Eq. (13) shows, the optimal policy p^* can be viewed as the reference policy p_{ref} whose actions are reweighted by a Boltzmann distribution $\exp(-\mathcal{E}(\cdot)/(\beta\mathcal{T}))$, and the reference policy p_{ref} performs bad due to limited real-world high-quality data, which is not the case in Ouyang et al. (2022); Rafailov et al. (2023); Wallace et al. (2023). Thus setting $1/\mathcal{T}$ to a sufficiently large constant can overcome the limitation of the pre-trained models as much as possible, in which case the preference regarding a pair of data becomes almost deterministic and the optimal policy approximately converges to the Boltzmann distribution, i.e., $p^*(\mathcal{R}^0) \propto \exp(-\mathcal{E}(\mathcal{R}^0)/(\beta\mathcal{T}))$.

D Implementation Details

D.1 Model Details

The architecture of the diffusion model used in our method is the same as Luo et al. (2022). The input of the model is the perturbed CDR-H3 and its surrounding context, i.e., 128 nearest residues of the antigen or the antibody framework around the residues of CDR-H3. The input is composed of single residue embeddings and pairwise embeddings. The single residue embedding encodes the information of its amino acid types, torsional angles, and 3D coordinates of all heavy atoms. The pairwise embedding encodes the Euclidean distances and dihedral angles between the two residues. The sizes of the single residue feature and the residue-pair features are 1285 and 64, respectively. Then the features are processed by Multiple Layer Perceptrons (MLPs). The number of layers is 6. The size of the hidden state in the layers is 128. The output of the model is the predicted categorical distribution of amino acid types, C_α coordinates, a $so(3)$ vector for the rotation matrix.

The number of diffusion steps is 100. We use the cosine β schedule with $s = 0.01$ suggested in Ho et al. (2020) for amino acid types, C_α coordinates, and orientations.

D.2 Training Details

Pre-training. Following Luo et al. (2022), the diffusion model is first trained via the gradient descent method Adam (Kingma & Ba, 2014) with `init_learning_rate=1e-4`, `betas=(0.9, 0.999)`, `batch_size=16`, and `clip_gradient_norm=100`. During the training phase, the weight of rotation loss, position loss, and sequence loss are each set to 1.0. We also schedule to decay the learning rate multiplied by a factor of 0.8 and a minimum learning rate of $5e-6$. The learning rate is decayed if there is no improvement for the validation loss in 10 evaluations. The evaluation is performed for every 1000 training steps. We trained the model on one NVIDIA GeForce GTX A100 GPU, and it could converge within 30 hours and 200k steps.

Fine-tuning. For ABDPO fine-tuning, the pre-trained diffusion model is further fine-tuned via the gradient descent method Adam with `init_learning_rate=1e-6`, `betas=(0.9, 0.999)`, and `clip_gradient_norm=100`. The batch size is 32. More specifically, in a batch, there are 16 pairs of energy-based preference data. We do not use decay learning rate and do not use weight decay in the fine-tuning process. And we use $\beta = 0.001$ in Eq. (8). We use the hyperparameter search space as follows. As for the energies introduced in Sec. 4.1, we use 1:2:1 or 1:2:2 to reweight them (i.e., CDR E_{total} , CDR-Ag E_{nonRep} , and CDR-Ag E_{Rep}). In practice, these four settings perform similarly in most cases. We fine-tune the pre-trained diffusion model for 20k steps for each antigen, separately.

D.3 Ranking Strategy

To rank the numerous generated antibodies with multiple energy labels, we applied a simple ranking strategy based on single energy metrics. The CDR E_{total} and the CDR-Ag ΔG of each antibody are ranked independently. Then, a composite ranking score for each antibody is defined as the sum of its CDR E_{total} rank and CDR-Ag ΔG rank. Finally, the antibodies are ranked according to these composite scores. We acknowledge that this ranking strategy has several limitations. For instance:

1. Equal weights are assigned to all energy types, despite them having differing importance in reality.
2. The distribution patterns of different energy types can vary, with these distributions usually being non-uniform. This

could result in scenarios where minor numerical differences in the top-ranking CDR-Ag ΔG values coincide with larger differences in CDR E_{total} , potentially leading to the selection of samples with suboptimal CDR E_{total} .

However, addressing these issues would require extensive and in-depth exploration of antibody binding mechanisms and energy calculation methodologies. We chose this straightforward, yet impartial, ranking strategy for two key reasons:

1. The primary goal of this work is to reformulate the antibody design task as an energy-focused optimization problem and propose a feasible implementation, rather than to delve into the mechanisms of antibody-antigen binding;
2. Our approach is designed to avoid introducing statistical biases or preference based on potentially erroneous prior knowledge or favoritism towards particular antibody design methods.

E Full Evaluation Results

E.1 Detailed Evaluation Results for Ranked Top-1 Design

In Tab. 1, we have reported the main results of ranked top-1 antibodies designed by our method and other baselines (refer to the ranking strategy in Appendix D.3). Here we will provide more detailed evaluation results for the ranked top-1 design as follows.

More Evaluation Metrics. To show more comprehensive results about the interaction between the antigens and the designed antibodies, we additionally evaluated CDR-Ag E_{nonRep} and CDR-Ag E_{Rep} along with CDR E_{total} and CDR-Ag ΔG . The evaluation results are reported in Tab. 6. As the results show, most of the baselines perform well in terms of CDR-Ag E_{nonRep} but fail in CDR-Ag E_{Rep} , which indicates the antibodies stay too close to the antigen. Our method can simultaneously achieve low CDR-Ag E_{nonRep} and low CDR-Ag E_{Rep} . This means that the antigen-antibody complex has almost no clashes and high binding affinity.

Detailed Performance for Each Antigen. In Tab. 11, we list the CDR E_{total} , CDR-Ag E_{nonRep} , CDR-Ag E_{Rep} , and CDR-Ag ΔG of the reference antibody in RAbD and the ranked top-1 antibodies designed by HERN, MEAN, dyMEAN, DiffAb, and ABDPO for each antigen in the test set separately. To more visually present the performance improvement of ABDPO over DiffAb, we also provided the detailed model performance comparison in Figs. 8 to 10. The results show that the ranked top-1 antibodies are effectively optimized in both CDR E_{total} and CDR-Ag ΔG in most cases.

Success Rates under Different Thresholds. In practice of drug discovery, antibodies with both rational structures and high binding affinity are desired. To show the ability of designing antibodies with both low CDR E_{total} and low CDR-Ag ΔG , we evaluate the *Success Rates* under different thresholds. The thresholds are computed as the 95% / 90% / 85% / 80% / 75% / 70% / 65% / 60% / 55% / 50% percentile of the CDR E_{total} and CDR-Ag ΔG of the real antibodies in the training set. The thresholds derived from different quantiles are shown in Tab. 4. Only if the CDR E_{total} and CDR-Ag ΔG of an antibody are both lower than the thresholds, it is viewed as a successful one. The corresponding results of ranked top-1 design of our method and other baselines are reported in Tab. 5. Among these approaches, our method achieves the best result under all thresholds.

Table 4. Different quantiles of metrics of the real antibodies in the training set. These quantiles are used for Success Rate thresholds. The unit, kcal/mol, is omitted for brevity.

Metric	95%	90%	85%	80%	75%	70%	65%	60%	55%	50%
CDR E_{total}	197.28	108.50	81.38	65.90	54.00	45.09	36.79	30.68	24.23	18.90
CDR-Ag ΔG	17.56	3.91	0.24	-0.82	-2.31	-3.98	-5.34	-6.38	-7.51	-8.78

Table 5. Success Rates of ranked top-1 antibodies designed under different thresholds. % is omitted for brevity.

Method	95%	90%	85%	80%	75%	70%	65%	60%	55%	50%
Reference	100.00	100.00	94.55	92.73	90.91	87.27	76.36	70.91	60.00	60.00
HERN	0.00	0.00	0.00	0.00	0.00	0.00	0.00	0.00	0.00	0.00
MEAN	0.00	0.00	0.00	0.00	0.00	0.00	0.00	0.00	0.00	0.00
dyMEAN	3.64	0.00	0.00	0.00	0.00	0.00	0.00	0.00	0.00	0.00
dyMEAN*	1.82	0.00	0.00	0.00	0.00	0.00	0.00	0.00	0.00	0.00
DiffAb	56.36	23.64	18.18	14.55	10.91	3.64	0.00	0.00	0.00	0.00
AbDPO	78.18	40.00	34.55	27.27	16.36	9.09	3.64	1.82	0.00	0.00

E.2 Evaluation Results for All Designs

We also provide evaluation results for all antibodies designed by our method as well as other baselines without ranking and selection in Tab. 7. We also provide the Success Rates under different thresholds in Tab. 8. In general, our approach

Antigen-Specific Antibody Design via Direct Energy-based Preference Optimization

Table 6. Summary of CDR E_{total} , CDR-Ag E_{nonRep} , CDR-Ag E_{Rep} , and CDR-Ag ΔG (kcal/mol) of reference antibodies and ranked top-1 antibodies designed by our model and other baselines. (\downarrow) denotes a smaller number is better.

Method	CDR E_{total} (\downarrow)		CDR-Ag E_{nonRep}		CDR-Ag E_{Rep}		CDR-Ag ΔG (\downarrow)	
	Avg.	Med.	Avg.	Med.	Avg.	Med.	Avg.	Med.
Reference	4.52	-1.33	-17.08	-18.24	6.11	4.78	-13.72	-14.54
HERN	7594.94	7825.92	-6.56	-4.57	2119.83	17.35	1159.34	4.12
MEAN	3113.7	2583.48	-6.17	-4.87	220.28	3.11	114.98	-0.92
dyMEAN	15025.67	7426.40	-13.23	-7.55	4371.34	395.29	2391.00	213.77
dyMEAN*	3234.30	1690.91	-13.57	-8.86	2968.75	331.09	1619.24	177.08
DiffAb	211.00	155.77	-4.82	-4.59	26.11	4.40	9.54	-1.97
AbDPO	162.75	124.62	-6.90	-6.26	3.72	1.47	-4.85	-5.24

outperforms others by a large margin.

Table 7. Summary of CDR E_{total} , CDR-Ag E_{nonRep} , CDR-Ag E_{Rep} , and CDR-Ag ΔG (kcal/mol) of all antibodies designed by our model and other baselines. Note that the ranking and selection procedures are not applied. (\downarrow) denotes a smaller number is better.

Method	CDR E_{total} (\downarrow)		CDR-Ag E_{nonRep}		CDR-Ag E_{Rep}		CDR-Ag ΔG (\downarrow)	
	Avg.	Med.	Avg.	Med.	Avg.	Med.	Avg.	Med.
HERN	10930.68	10776.79	-10.9	-5.32	3656.77	569.61	2000.32	306.79
MEAN	7138	6011.53	-9.34	-6.82	1903.32	907.69	1037.49	491.49
dyMEAN	17302.98	8157.17	-14.94	-7.46	5411.50	893.88	2961.39	484.09
dyMEAN*	4078.22	2238.42	-16.20	-10.73	4240.43	1415.49	2316.04	769.99
DiffAb	1592.73	1340.42	-9.10	-7.33	2168.43	1212.86	1183.54	658.39
AbDPO	989.59	634.34	-6.19	-4.61	513.53	32.93	276.25	12.95

Table 8. Success Rates of all antibodies designed by our model and other baselines under different thresholds. Note that the ranking and selection procedures are not applied. % is omitted for brevity. A cell shaded in green within the table represents at least one successful antibody, with the row indicating the specific method used, and the column designating the particular thresholds applied.

Method	95%	90%	85%	80%	75%	70%	65%	60%	55%	50%
HERN	0.00	0.00	0.00	0.00	0.00	0.00	0.00	0.00	0.00	0.00
MEAN	0.00	0.00	0.00	0.00	0.00	0.00	0.00	0.00	0.00	0.00
dyMEAN	0.95	0.00	0.00	0.00	0.00	0.00	0.00	0.00	0.00	0.00
dyMEAN*	1.40	0.00	0.00	0.00	0.00	0.00	0.00	0.00	0.00	0.00
DiffAb	2.28	0.80	0.34	0.14	0.04	0.01	0.00	0.00	0.00	0.00
AbDPO	13.05	5.02	2.36	1.00	0.41	0.10	0.02	0.00	0.00	0.00

E.3 Involving Rosetta Structure Optimization

To further explore the potential of ABDPO, we introduce structure optimization into our framework. More specifically, we use the energy after structure optimization in Rosetta (Alford et al., 2017) to determine the preference instead of that directly evaluated on the structure generated by the diffusion model. Due to the expensive computation cost of structure optimization, we randomly select 8 antigens in the test set. We use DiffAb with Rosetta structure optimization as the baseline. Due to the randomness in Rosetta structure optimization, we evaluate metrics over all synthetic antibodies instead of the ranked top-1 antibody. The evaluation results are reported in Tab. 9. We also compute the Success Rates under different thresholds as in Appendix E.1 and report the results in Tab. 10. These results are promising and show the consistent superiority of our framework. Notably, even at the strict thresholds that correspond to the 50-th percentile, ABDPO with Rosetta structure optimization has a certain success rate in all cases while DiffAb cannot design qualified antibodies at all in some cases.

In many cases, antibodies designed by ABDPO with Rosetta structure optimization have comparable performance with real antibodies. Here we provide a visualization of a case (antigen PDB ID: 1ncb) in Fig. 11.

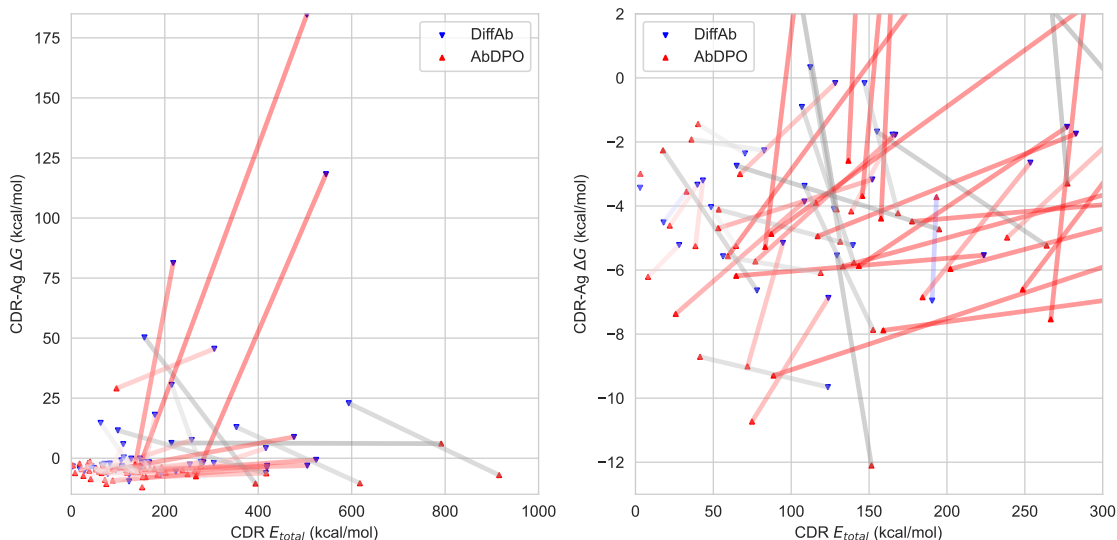


Figure 8. Performance comparison of DiffAb and ABDPO. Each point refers to an antibody designed by DiffAb and ABDPO for a specific antigen and has a unique correspondence in Tab. 11. The x-coordinate (resp. y-coordinate) of a point represents the CDR E_{total} (resp. CDR-Ag ΔG) of the antibody. For a specific antigen, we draw a line connecting the points that represent the antibody designed by DiffAb and ABDPO to show the change of metrics. If both metrics are improved, the line is plotted in red. If only one metric is improved, the line is plotted in blue. Otherwise, the line is plotted in black. To visually present the degree of the change, the magnitude of the change corresponds proportionally to the intensity of the line's coloration.

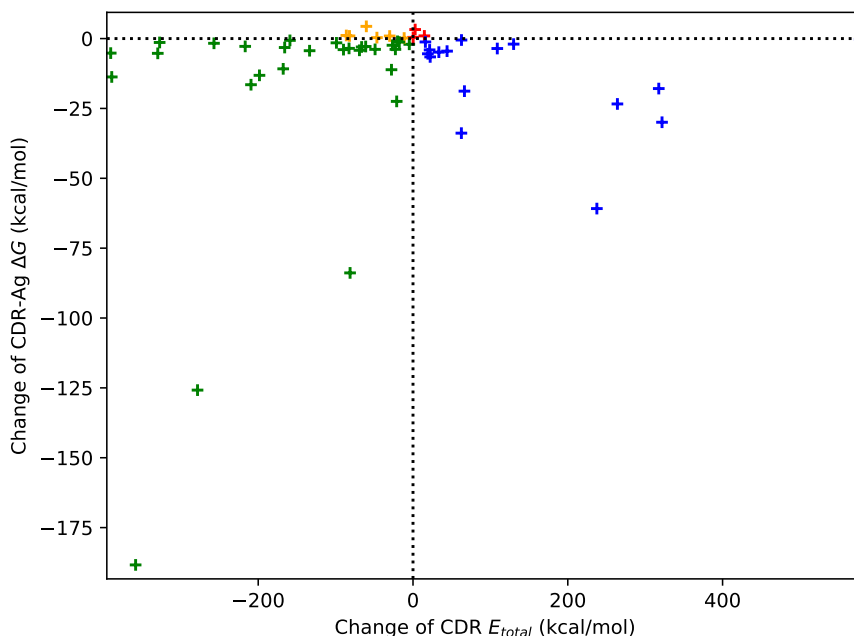


Figure 9. Difference in CDR E_{total} and CDR-Ag ΔG of the ranked top-1 antibody designed by ABDPO and DiffAb. Each point refers to a specific antigen. The x-coordinate (resp. y-coordinate) represents the difference in CDR E_{total} (resp. CDR-Ag ΔG). The color of the point depends on the quadrant in which it is located. The point located in the First/Second/Third/Fourth Quadrant is plotted in red/orange/green/blue, respectively.

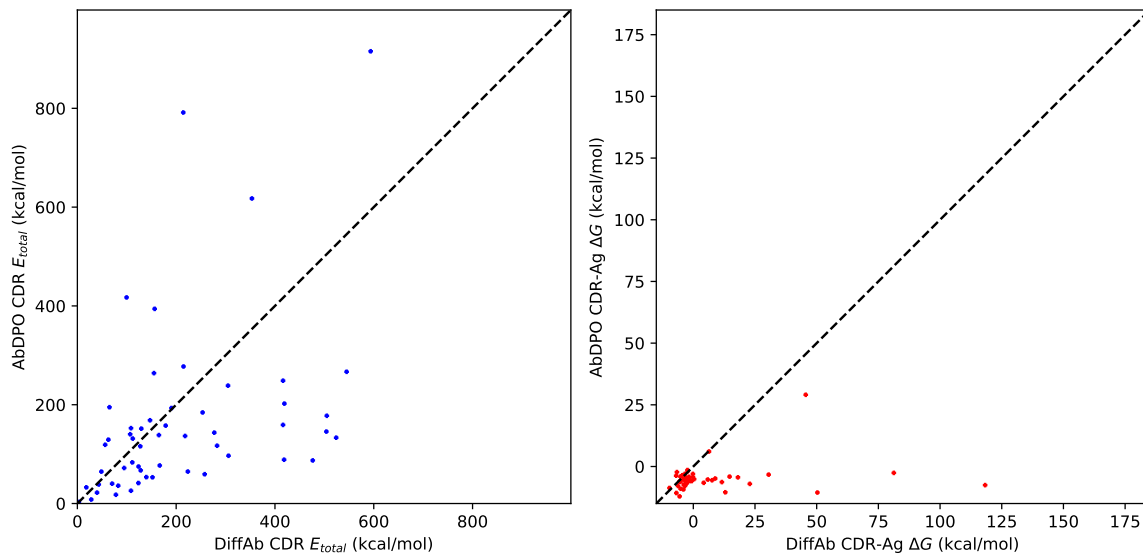


Figure 10. Performance comparison of the ranked top-1 antibodies designed by DiffAb and ABDPO for each antigen in the test set in terms of CDR E_{total} (left) and CDR-Ag ΔG (right). Its x-coordinate and y-coordinate of a point represent the performance of DiffAb and ABDPO in the same antigen, respectively.

Table 9. Summary of CDR E_{total} and CDR-Ag ΔG (kcal/mol) of antibodies designed by DiffAb and ABDPO with Rosetta Structure Optimization. (\downarrow) denotes a smaller number is better.

PDB ID	DiffAb + Rosetta Structure Optimization					ABDPO + Rosetta Structure Optimization				
	CDR E_{total} (\downarrow)		CDR-Ag ΔG (\downarrow)		Success Rate (\uparrow)	CDR E_{total} (\downarrow)		CDR-Ag ΔG (\downarrow)		Success Rate (\uparrow)
	Avg.	Med.	Avg.	Med.		Avg.	Med.	Avg.	Med.	
1ncb	61.59	59.04	-0.00	0.19	0%	26.29	18.86	-5.62	-5.36	3.23%
2xwt	41.84	35.25	-3.38	-2.97	0%	15.81	13.64	-4.99	-5.21	6.25%
1iqd	54.84	36.16	-2.34	-2.96	6.45%	9.78	1.84	-6.00	-6.20	12.5%
1a14	19.32	16.72	-4.19	-4.50	3.12%	16.20	11.60	-3.32	-2.82	6.25%
5ggs	42.98	36.07	-1.93	-2.24	0%	17.77	7.77	-5.57	-6.08	12.9%
4ki5	23.81	19.74	-5.19	-5.47	10%	10.19	7.00	-6.98	-7.39	20%
4cmh	67.89	67.11	4.99	2.47	0%	20.90	14.16	-5.98	-6.11	22.58%
3hi6	48.29	47.62	-1.82	-1.84	0%	20.21	11.83	-7.71	-8.01	18.75%

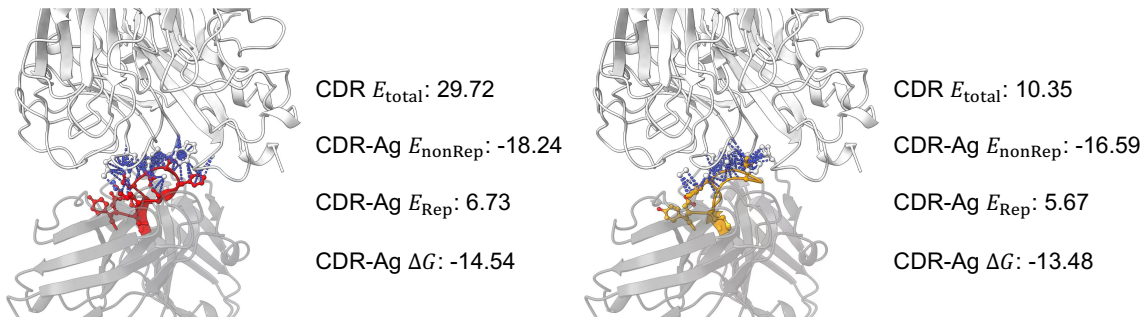


Figure 11. Examples of the reference antibody (left) and an antibody designed by ABDPO with Rosetta structure optimization (right) for the antigen whose PDB ID is 1ncb.

Table 10. Success Rates under different thresholds (see Tab. 4) of DiffAb and AbDPO with Rosetta structure optimization. % is omitted for brevity. A cell shaded in red within the table represents that all antibodies fail to pass the thresholds, with the row indicating the specific antigen, and the column designating the particular thresholds applied.

PDB ID	Method	95%	90%	85%	80%	75%	70%	65%	60%	55%	50%
1ncb	DiffAb	96.88	84.38	43.75	34.38	28.12	18.75	12.50	6.25	0.00	0.00
	AbDPO	100.00	100.00	90.32	83.87	80.65	58.06	29.03	16.13	9.68	3.23
2xwt	DiffAb	100.00	90.00	80.00	63.33	56.67	40.00	20.00	13.33	6.67	0.00
	AbDPO	100.00	100.00	96.88	96.88	84.38	65.62	40.62	18.75	9.38	6.25
1iqd	DiffAb	93.55	87.10	64.52	51.61	45.16	29.03	25.81	12.90	9.68	6.45
	AbDPO	100.00	100.00	100.00	96.88	93.75	71.88	56.25	31.25	18.75	12.50
1a14	DiffAb	100.00	100.00	100.00	81.25	71.88	59.38	31.25	15.62	9.38	3.12
	AbDPO	100.00	100.00	100.00	81.25	59.38	21.88	15.62	9.38	9.38	6.25
5ggs	DiffAb	100.00	86.67	60.00	53.33	36.67	16.67	10.00	3.33	0.00	0.00
	AbDPO	100.00	100.00	90.32	90.32	80.65	70.97	45.16	35.48	22.58	12.90
4ki5	DiffAb	100.00	100.00	93.33	90.00	73.33	56.67	40.00	23.33	16.67	10.00
	AbDPO	100.00	100.00	100.00	96.67	86.67	76.67	66.67	60.00	36.67	20.00
4cmh	DiffAb	86.67	60.00	33.33	16.67	13.33	10.00	6.67	3.33	0.00	0.00
	AbDPO	100.00	96.77	90.32	83.87	74.19	67.74	54.84	41.94	38.71	22.58
3hi6	DiffAb	100.00	90.00	66.67	56.67	40.00	20.00	13.33	6.67	3.33	0.00
	AbDPO	100.00	96.88	96.88	93.75	87.50	75.00	53.12	43.75	37.50	18.75

F Extended Ablation Studies

Due to the massive training cost in the RAbD benchmark, we investigate the effectiveness and necessity of each proposed component on five representative antigens, whose PDB IDs are 1a14, 2dd8, 3cx5, 4ki5, and 5mes. From the results in Fig. 12, it is clear that ABDPO can significantly boost the overall performance of ablation cases. Note that moving averages are applied to smooth out the curves to help in identifying trends, including Fig. 4. We present observations and constructive insights of the three proposed components as follows:

1. The residue-level DPO is vital for training stability specifically for CDR E_{total} . As aforementioned in Section 3.2, the residue-level DPO implicitly provides fine-grained and rational gradients. In contrast, vanilla DPO (without residue-level DPO) may impose unexpected gradients on stable residues, which incurs the adverse direction of optimization. According to each energy curve in Figure 12, we observe that residue-level DPO surpasses vanilla DPO at least one energy term.
2. Without Energy Decomposition, all five cases appear undesired “shortcuts” aforementioned in Section 3.3. We observe that the energy of CDR E_{total} exhibits a slight performance improvement over the ABDPO after the values of attraction and repulsion reach zero. We suppose that is the result of the combined effects of low attraction and repulsion. Because the generated CDR-H3 is far away from the antigen in this case, the model can concentrate on refining CDR E_{total} without the interference of attraction and repulsion.
3. The Gradient Surgery can keep a balance between attraction and repulsion. We can see the curves of CDR-Ag E_{nonRep} are consistently showing a decline, while the curves of CDR-Ag E_{Rep} are showing an increase. This observation verifies that ABDPO without Gradient Surgery is unable to optimize CDR-Ag E_{nonRep} and CDR-Ag E_{Rep} simultaneously. Additionally, the increase in attraction significantly impacts the repulsion, causing the repulsion to fluctuate markedly.

G Limitations and Future Work

Diffusion Process of Orientations. As Luo et al. (2022) stated and we have mentioned in Sec. 3.1, Eq. (1) is not a rigorous diffusion process. Thus the loss in Eq. (7) cannot be rigorously derived from the KL-divergence in Eq. (4), though they share the idea of reconstructing the ground truth data by prediction. However, due to the easy implementation and fair comparison with the generative baseline, i.e., DiffAb (Luo et al., 2022), we adopt Eq. (7) in the ABDPO loss in Eq. (8). In practice, we empirically find that it works well. FrameDiff (Yim et al., 2023), a protein backbone generation model, adopts a noising process and a rotation loss that are well compatible with the theory of score-based generative models (also known as diffusion models). In the future, we modify the diffusion process of orientations as Yim et al. (2023) for potential further improvement.

Energy Estimation. In this work, we utilize Rosetta/pyRosetta to calculate energy, although it is already one of the most authoritative energy simulation software programs and widely used in protein design and structure prediction, the final energy value is still difficult to perfectly match the actual experimental results. In fact, any computational energy simulation software, whether it is based on force field methods such as OpenMM (Eastman et al., 2017) or statistical methods like the Miyazawa-Jernigan potential (Miyazawa & Jernigan, 1985), will exhibit certain biases and cannot fully simulate reality. An in vitro experiment is the only way to verify the effectiveness of the designed antibodies. However, due to the significant amount of time consumed by in vitro experiments and considering that the main goal of our work is to propose a novel view of antibody design, we did not perform the in vitro experiment.

Future Work on Preference Definition. The preference used in ABDPO determine the tendency of antibody generation, and we will strive to continue exploring the definition of preference to more closely align the antibody design process with the real-world environment of antibody activity. Further, we aim to synchronize the preference with the outcomes of in vitro experiments and expect that our method will ultimately generate effective antibodies in real-world applications. The exploration of preference can be divided into two aspects: enhancing existing preference and integrating new components or energies.

1. Improvements to current preference: (1) performing more fine-grained calculations on the current three types of energy, such as decomposing CDR E_{total} into interactions between the CDR and the rest of the antibody, interactions within the CDR, and energy at the single amino acid level; (2) exploring the varying importance of preferences for antibodies and determining the relative weights of each preference during the optimization and ranking of generated antibodies.
2. The introduction of new components or energies is intended to address additional challenges in antibody engineering, focusing on aspects such as antibody stability, solubility, immunogenicity, and expression level. Additionally, we consider integrating components that target antibody specificity.

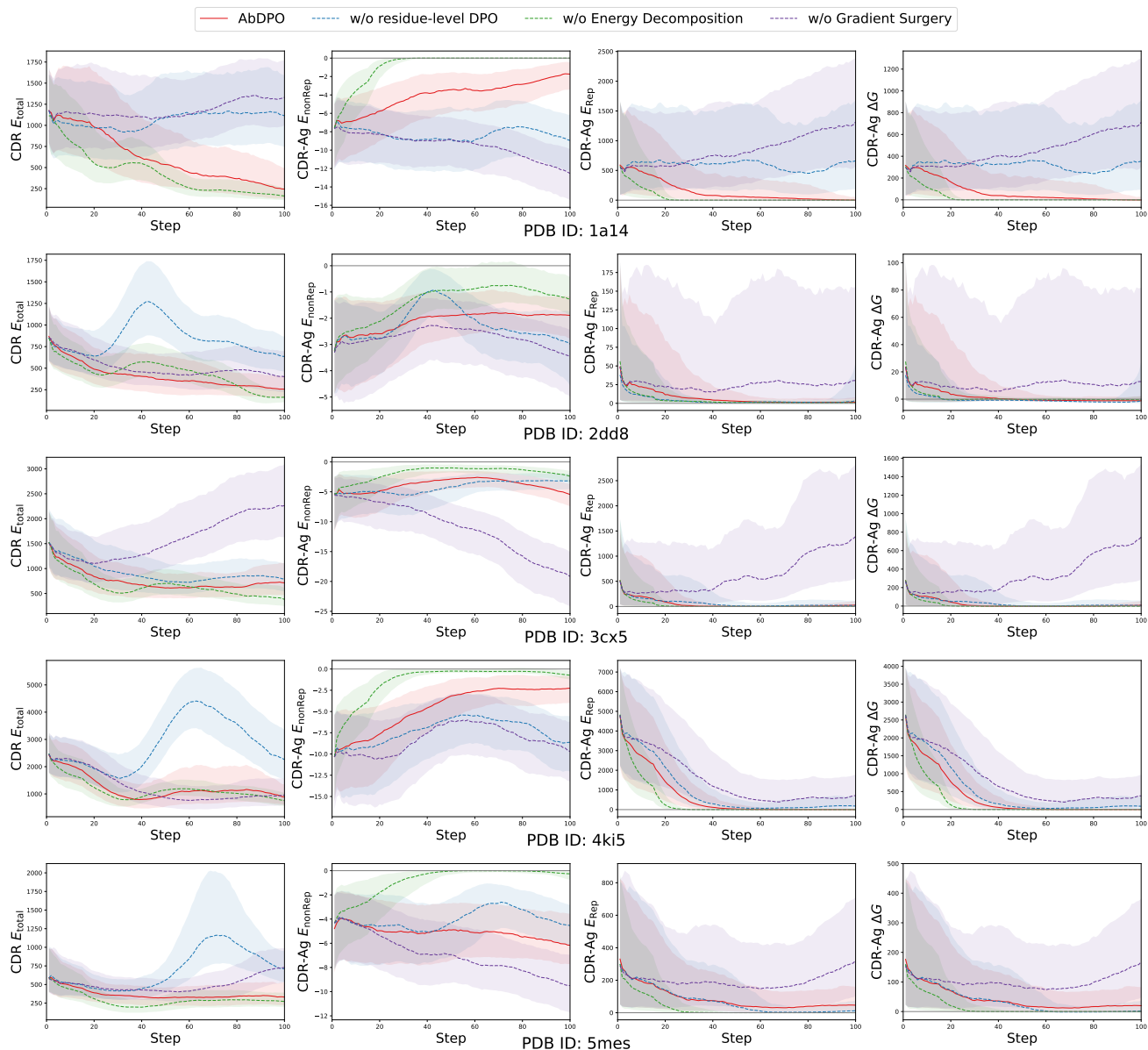


Figure 12. Changes of median CDR E_{total} , CDR-Ag E_{nonRep} , CDR-Ag E_{Rep} , and CDR-Ag ΔG (kcal/mol) over optimization steps, shaded to indicate interquartile range (from 25-th percentile to 75-th percentile). The rows represent PDB 1a14, 2dd8, 3cx5, 4ki5, and 5mes respectively, in a top-down order.